Side feeding patterns and nuclear lifetime determinations by the Doppler shift attenuation method in $(\alpha,n\gamma)$ reactions

C. Mihai,[1,*] A. A. Pasternak,[2] D. Filipescu,[1] M. Ivaşcu,[1] D. Bucurescu,[1] G. Căta-Danil,[1] I. Căta-Danil,[1] D. Deleanu,[1] D. Ghiţă,[1] T. Glodariu,[1] Yu. N. Lobach,[3] N. Mărginean,[1] R. Mărginean,[1] A. Negret,[1] S. Pascu,[1] T. Sava,[1] L. Stroe,[1] G. Suliman,[1] and N. V. Zamfir[1]

[1]*Horia Hulubei National Institute of Physics and Nuclear Engineering, R-76900 Bucharest, Romania*

[2]*Cyclotron Laboratory, A.F. Ioffe Physical Technical Institute, RV-194021 St. Petersburg, Russia*

[3]*Institute for Nuclear Research UAS, pr. Nauki 47, 252028 Kiev, Ukraine*

(Received 5 January 2010; published 29 March 2010)

γ rays were measured at several angles in both singles and coincidence mode in the ^{119}Sn$(\alpha,n\gamma)^{122}$Te reaction at 15 MeV on a thick target. Lifetimes of excited states in ^{122}Te were determined from a Monte Carlo Doppler shift attenuation method (DSAM) analysis of the Doppler broadened lines shapes of γ rays de-exciting the levels. A comparison of several deduced lifetimes with recent results obtained with the (n,n') reaction allowed us to validate the choice of a parameter used to calculate the contribution of the side feeding times. The ingredients of the DSAM line-shape analysis (stopping power, description of instrumental line shapes, and side feeding evaluation) are presented in some detail. It is concluded that with proper treatment of side feeding, a DSAM line-shape analysis of peaks in singles or coincidence spectra obtained following the $(\alpha,n\gamma)$ reaction is able to provide rather accurate values for the lifetimes of levels with low and medium spins.

DOI: 10.1103/PhysRevC.81.034314 PACS number(s): 21.10.Tg, 23.20.Lv, 25.55.Hp, 27.60.+j

I. INTRODUCTION

Measurement of the lifetimes of excited nuclear levels is a very important issue in nuclear spectroscopy, because these quantities are the essential ingredient in the determination of reduced electromagnetic transition rates, quantities that are rather sensitive to details of the intrinsic structure of these states. Most of the states at relatively low excitation energies (up to several megaelectronvolts) have lifetimes from tens of femtoseconds to 1–2 ps, which is the domain of applicability of the Doppler shift attenuation method (DSAM) [1]. The details of the DSAM analysis depend on the reaction used to populate the levels. If the recoil velocities are very low, such that the Doppler shifts of the de-exciting γ rays are much smaller than the energy resolution of the detector, one can only measure a shift of the average energy of the γ rays (the centroid method). If the Doppler shifts are comparable to or larger than the resolution, then one can determine the lifetimes by analyzing the Doppler broadened line shapes of the γ rays. Important ingredients in such an analysis are the reaction kinematics, the de-excitation process of the nucleus, the slowing-down of the recoils in the target material, and the geometry of the experimental setup.

The nuclear reaction used also determines which nuclear levels can be observed. Heavy-ion-induced fusion-evaporation reactions (HI,$xnypz\alpha\gamma$) strongly populate high-spin states along the yrast line and, with a reasonable intensity, also some yrare structures. At the other limit, reactions of the type $(p,n\gamma)$ or $(n,n'\gamma)$ populate nonselectively low-spin states. The (α, n) reaction is a special case that populates with reasonable intensity low- and medium-spin states in a larger spin window, both yrast and nonyrast: this reaction actually being considered as a tool for "complete spectroscopy" for such states [2]. This is the first advantage of using the (α,n) reaction rather than a heavy-ion-induced reaction: many nonyrast states of low spin, which can offer important structure information, can be studied only in this way. Another advantage of this reaction concerns the way the levels are fed in the reaction. The influence of cascade feeding (from discrete levels) is much smaller in this case. Also, the side feeding of the levels is mainly realized by fast statistical $E1$ transitions from the entry states in the continuum, which differs from the case of HI-induced reactions or even the $(\alpha,2n)$ reaction, where the feeding by slower cascades of stretched $E2$ transitions is significant. Finally, at the low beam energies necessary for (α,n) reactions, a very small number of other channels may be open [only the (α, p) or $(\alpha,2n)$ may compete in certain cases), so that one can easily obtain singles γ-ray spectra with high statistics and clean enough for line-shape analysis. Moreover, no new channels will be opened during the slowing-down process, therefore one can use thick targets [3].

However, a few disadvantages of the same (α,n) reaction must be noted, which lead to special requirements for such measurements. The first is the relatively low velocity of the recoils (typically $v/c \approx 0.3\%$), meaning that the Doppler effect is smaller than the FWHM energy resolution of a good HPGe detector even for a γ-ray energy of 1 MeV or even higher. Therefore, the instrumental line shape (the detector response) must be well measured to perform a meaningful line-shape analysis. Owing to the small Doppler effect and relatively low population of cascades above the transition of interest, it is impossible to apply well-known gating techniques used in HI reactions to avoid problems caused by cascade and side feedings, such as Flight Gate on the Transition Above or Narrow Gate on the Transition Below. Therefore, in our case, one must use reliable methods of

*cmihai@tandem.nipne.ro

estimation of the cascade and side feeding times. Finally, the nuclear component of the recoil stopping power dominates the electronic stopping power, which results in a fast slowing-down of the recoils in the target (typical stopping times t_s of <0.5 ps). Thus, measurements of lifetimes τ larger than 1 ps become rather difficult. On the contrary, even relatively short effective side feeding times (of the order of 0.1–0.2 ps) drastically influence the measured effects, which again emphasizes the importance of accurate side feeding pattern estimation.

In the present work we examine in detail the possibilities offered by DSAM analysis in the $(\alpha,n\gamma)$ reaction. To this end, we analyze data measured for the ^{119}Sn$(\alpha,n\gamma)^{122}$Te reaction and compare the results with other measurements, most notably with the rather complete lifetime measurements for low-spin states with the $(n,n'\gamma)$ reaction [4]. It is shown that, provided the cascade and side feedings are properly treated, rather accurate lifetime determinations are possible with this reaction for many states with spin up to $8\hbar$. Section II describes the experiment, and Sec. III reports the technical details of the DSAM analysis and its results.

II. EXPERIMENT

The experiment was performed at the Bucharest TANDEM Van de Graaf accelerator. The (α,n) reaction was performed on a thick ^{119}Sn target (4.3 mg/cm^2; much thicker than the range of recoils in the target, which is about 0.15 mg/cm^2), at an incident beam energy of 15 MeV. Typical beam currents on the target were in the range of 10 electrical nA. γ rays were measured with a small array of seven HPGe detectors, each with a relative efficiency of about 55%, placed at an average distance of 12 cm from the target. Both singles spectra and coincidences between all these detectors were recorded. Careful calibrations in both energy and efficiency were performed for all these detectors, using ^{133}Ba, ^{60}Co, and ^{152}Eu sources placed at the target position. Different $\gamma\gamma$ coincidence matrices were constructed, such as a symmetric one including all the detectors (used to place possible unknown transitions or new levels in the level scheme) and matrices in which events in one or more detectors were sorted against events in all detectors. Most detectors had an FWHM energy resolution of between 1.9 and 2.1 keV at 1.33 MeV. Five detectors were placed in the backward direction at an angle of 143° with respect to the beam (denoted b in the following), one was kept at 90° throughout (denoted p), and the last one was mobile, being placed at different angles in the forward direction (f): 10°, 37°, and 55°. One of the best detectors from the backward direction was used in the DSAM singles spectrum analysis. Thus, the summed forward spectra (f) had statistics comparable with those of the p and b spectra, which is important for the comparison of analyses of the Doppler broadened line shapes. Coincidence spectra, summed over all angles, were also used for the DSAM analysis.

Assignment of the γ rays in the spectra to transitions in the level scheme was performed both starting from the known level scheme [5] and on the basis of the results of the presently observed $\gamma\gamma$ coincidence relationships.

III. EXPERIMENTAL RESULTS AND ANALYSIS

A. The level scheme

We observed levels in ^{122}Te with spins up to $10\hbar$ and excitation energies up to ∼3.3 MeV. Because we observed a large number of excited levels, many levels with the same spin (e.g., six excited 2^+ states), and many transitions between all these levels, presentation of the observed level scheme in a graph would be too complicated. Therefore we present the complete results of the experiment in Table I. This table lists the assignments of the observed γ-ray transitions and their relative intensities (which determine the feeding relationships). This information is important for the DSAM analysis described in the following. The extracted lifetimes are discussed at the end. From coincidence relationships we placed in the level scheme a number of 25 new excited states with excitation energies from 2642 to 3685 keV (see Table I). On the basis of their decay transitions, one can deduce that the spin values of these levels are moderately high. The four new levels up to 2946 keV feed mainly 4^+ and 6^+ states. The new levels placed above 2950 keV feed mainly the 5^- state at 2407 keV, the 6^+ states at 1751 and 2284 keV, and the 8^+ level at 2670 keV. Figure 1 shows two $\gamma\gamma$ coincidence spectra with gates set on the $6_1^+ \rightarrow 4_1^+$ and $8_1^+ \rightarrow 6_1^+$ transitions, respectively: spectra in which transitions from many of the newly observed levels are highlighted. Except for the new levels and new transitions from the present work, the level energies in Table I were taken from Refs. [4] and [5]. The relative intensities of the transitions were extracted from the 55° singles spectrum, and for some weak transitions they were estimated from $\gamma\gamma$ coincidence spectra.

B. General considerations on the Doppler shift attenuation method analysis

Analysis of the experimental DSAM line shapes was carried out using updated versions of the Monte Carlo codes COMPA, GAMMA, and SHAPE, which are described in some detail in Refs. [6–8] and have been widely used for heavy-ion-induced reactions (some recent references are [9–11]). This software includes the Monte Carlo simulation for the production and slowing-down of recoils, as well as for γ-ray production and detection. In the COMPA program the reaction kinematics, the slowing-down of the projectiles in the target, the formation of the compound nuclei, the particle emission, and the entry-state population distributions are simulated. The GAMMA program simulates the slowing-down process and the multiple scattering of the recoils in the target, the emission of γ-ray cascades from the entry states to the level of interest, and the detection of γ quanta in the detector system. In the calculation of Doppler attenuated line shapes, the cascade feeding through all known levels is taken into account along with the side feeding cascades from each entry state. In the DSAM program the line shapes resulting from the experiment are fitted taking into account the instrumental line shapes of the detector. Up to seven overlapping peaks that may have Doppler broadening or only an instrumental shape can be simultaneously fitted by using lifetimes, positions, and relative areas as parameters.

TABLE I. Experimental information obtained in the present study of the ^{119}Sn(α,$n\gamma$)^{122}Te reaction at 15 MeV. Except for newly assigned excited states, level energies given are taken from Refs. [4] and [5]. γ-ray energies are given as measured in the present experiment.

E_x (keV)	I^π	E_γ	E_f	I_f^π	Int.
564.12(1)	2^+	564.09(1)	0	0^+	1000
1181.23(7)	4^+	617.22(1)	564.12(1)	2^+	524.5(60)
1256.83(4)	2^+	692.79(1)	564.12(1)	2^+	128.7(28)
		1256.84(4)	0	0^+	24.4(6)
1357.3(1)	0^+	793.13(2)	0	0^+	14.7(5)
1746.99(7)	0^+	490.26(5)	1256.83(4)	2^+	1.5(3)
		1182.3(1)	564.12(1)	2^+	1.9(5)
1750.91(9)	6^+	569.97(1)	1181.23(7)	4^+	148.6(20)
1752.60(5)	2^+	395.19(2)	1357.3(1)	0^+	1.9(2)[a]
		495.43(3)	1256.83(4)	2^+	2.35(34)
		1188.5(1)	564.12(1)	2^+	7.3(7)[a]
		1752.6(3)	0	0^+	19.2(8)
1909.50(5)	4^+	652.69(3)	1256.83(4)	2^+	7.4(3)
		728.29(5)	1181.23(7)	4^+	35.1(7)
		1345.6(1)	564.12(1)	2^+	23.5(6)
1940.01(7)	0^+	683.63(2)	1256.83(4)	2^+	4.1(8)
		1376.02(2)	564.12(1)	2^+	0.17(5)[b]
1951.68(5)	3^+	695.09(2)	1256.83(4)	2^+	32.5(10)
		770.61(2)	1181.23(7)	4^+	10.8(8)
		1387.8(2)	564.12(1)	2^+	18.7(6)
2041.07(6)	4^+	784.1(1)	1256.83(4)	2^+	1.6(4)[a]
		859.87(2)	1181.23(7)	4^+	16.3(5)
		1477.1(2)	564.12(1)	2^+	15.0(5)
2099.22(6)	2^+	1535.4(2)	564.12(1)	2^+	17.3(6)
		2098.88(35)	0	0^+	0.65(6)[b]
2196.80(4)	3^-	939.92(6)	1256.83(4)	2^+	0.03(1)[b]
		1015.3(1)	1181.23(7)	4^+	1.9(4)[a]
		1632.9(5)	564.12(1)	2^+	22.3(8)
2203.75(5)	1	946.77(12)	1256.83(4)	2^+	0.44(5)[b]
		1639.8(5)	564.12(1)	2^+	4.5(3)
		2203.58(10)	0	0^+	1.3(1)[b]
2283.45(7)	6^+	532.79(1)	1750.91(9)	6^+	19.6(5)
		1102.72(5)	1181.23(7)	4^+	17.5(6)
2287.36(5)	2^+	1030.18(15)	1256.83(4)	2^+	0.50(4)[b]
		1105.50(50)	1181.23(7)	4^+	0.2(2)[b]
		1723.9(5)	564.12(1)	2^+	8.4(4)
		2287.52(15)	0	0^+	0.88(7)[b]
2310.68(5)	2^+	557.82(5)	1752.60(5)	2^+	0.42(13)[b]
		953.05(16)	1357.3(1)	0^+	0.41(4)[b]
		1129.64(24)	1181.23(7)	4^+	0.35(3)[b]
		1747.1(5)	564.12(1)	2^+	9.4(6)
2407.12(9)	5^-	1226.2(4)	1181.23(7)	4^+	36.5(11)
2407.96(5)	2^+	1844.4(5)	564.12(1)	2^+	7.0(5)
2448.47(5)	$(4)^+$	539.01(3)[e]	1909.50(5)	4^+	0.9(3)[a]
		1267.3(3)	1181.23(7)	4^+	21.6(14)
		1884.27(12)	564.12(1)	2^+	2.0(2)[b]
2535.68(9)	5	626.28(9)[e]	1909.50(5)	4^+	1.5(2)[a]
		784.41(3)[e]	1750.91(9)	6^+	1.4(3)[a]
		1354.4(3)	1181.23(7)	4^+	14.2(6)
2538.58(4)	4^-	586.94(1)	1951.68(5)	3^+	12.7(6)
		629.31(2)	1909.50(5)	4^+	1.9(3)[a]
		1357.3(3)	1181.23(7)	4^+	4.1(3)
2557.74(7)	2,3	1301.1(1)	1256.83(4)	2^+	9.0(2)[a]
2560.38(21)	2^+,3,4,5	1379.3(1)	1181.23(7)	4^+	10.8(9)[a]
2600.78(6)	3	1419.2(2)	1181.23(7)	4^+	5.1(2)[a]

TABLE I. *(Continued.)*

E_x (keV)	I^π	E_γ	E_f	I_f^π	Int.
		2036.57(12)	564.12(1)	2^+	2.49(11)[b]
2603.74(14)	4	1422.4(1)	1181.23(7)	4^+	6.5(2)[a]
2636.01(5)	(1,2,3)	1379.2(1)	1256.83(4)	2^+	6.8(5)[a]
		2072.16(15)	564.12(1)	2^+	1.26(14)[b]
2642.8(2)[d]		602.22(2)[e]	2041.07(6)	4^+	1.9(2)[a]
		733.47(5)[e]	1909.50(5)	4^+	2.7(6)[a]
		891.90(5)[e]	1750.91(9)	6^+	4.3(3)[a]
2654.39(6)	2,3	1397.9(1)	1256.83(4)	2^+	5.8(7)
		2091.00(36)	564.12(1)	2^+	1.2(2)[b]
2669.04(6)	3^+	1488.0(1)	1181.23(7)	4^+	5.9(6)
		2104.96(15)	564.12(1)	2^+	1.15(12)[b]
2669.78(14)	8^+	918.42(2)	1750.91(9)	6^+	15.2(5)
2679.39(6)	4^+	1422.5(2)	1256.83(4)	2^+	1.5(3)[a]
		2116.02(25)	564.12(1)	2^+	3.6(7)[b]
2693.57(6)	4^+	1436.59(39)	1256.83(4)	2^+	0.53(5)[b]
		1512.3(2)	1181.23(7)	4^+	6.7(5)
2758.30(11)	$5(^+)$	717.51(2)	2041.07(6)	4^+	0.3(2)[a]
		1576.8(2)	1181.23(7)	4^+	6.7(6)[a]
2758.75(9)	(6^-)	351.47(1)	2407.12(9)	5^-	7.2(4)
		1007.3(1)	1750.91(9)	6^+	3.5(4)
2770.47(9)	3,4,5	1589.9(4)	1181.23(7)	4^+	7.4(7)
2772.45(8)	2^+,3,4,5	1591.9(4)	1181.23(7)	4^+	7.9(7)
2800.82(10)	7^-	393.2(2)	2407.12(9)	5^-	0.57(7)[c]
		1049.3(1)	1750.91(9)	6^+	10.8(4)
2809.99(7)	4^+,3	1628.6(2)	1181.23(7)	4^+	3.5(5)[a]
		2245.51(19)	564.12(1)	2^+	0.31(7)[b]
2816.69(7)	4,5	907.06(10)	1909.50(5)	4^+	1.1(2)[a]
		1635.9(2)	1181.23(7)	4^+	4.6(5)[a]
2837.47(4)		1657.6(4)	1181.23(7)	4^+	3.0(4)[a]
2860.48(6)		1679.5(3)	1181.23(7)	4^+	7.5(4)
2878.3(2)[d]		1127.4(2)[e]	1750.91(9)	6^+	7.0(4)[a]
2889.7(10)		606.6(1)	2283.45(7)	6^+	0.4(2)[a]
		1138.8(3)	1750.91(9)	6^+	4.7(3)[a]
2900.3(2)[d]		451.87(3)[e]	2448.47(5)	$(4)^+$	1.7(3)[a]
2901.05(11)	$5^{(-)}$,(4)	1719.9(2)	1181.23(7)	4^+	2.0(3)[a]
2913.5(4)	(8^+)	629.5(3)[e]	2283.45(7)	6^+	0.3(2)[a]
		1161.8(1)	1750.91(9)	6^+	8.2(4)
2930.65(7)	4,5	733.42(8)	2196.80(4)	3^-	1.6(3)[b]
		1750.5(3)	1181.23(7)	4^+	4.6(5)[a]
2946.3(1)[d]		1765.2(2)[e]	1181.23(7)	4^+	3.6(2)[a]
2958.01(10)	4^+,3	1701.48(47)	1256.83(4)	2^+	1.13(11)[b]
		1774.4(4)	1181.23(7)	4^+	3.9(3)[a]
		2393.79(26)	564.12(1)	2^+	2.4(2)[b]
2960.7(3)[d]		553.6(1)[e]	2407.12(9)	5^-	2.0(2)[a]
		1051.6(1)[e]	1909.50(5)	4^+	0.5(2)[a]
2971.88(12)	(7^-)	687.79(2)	2283.45(7)	6^+	0.7(2)[a]
		1220.34(8)	1750.91(9)	6^+	2.8(3)[a]
2975.43(14)	2,3,4	568.02(11)[e]	2407.12(9)	5^-	1.9(2)[a]
		778.64(8)	2196.80(4)	3^-	2.0(3)
2993.54(8)	4^+	1736.18(30)	1256.83(4)	2^+	0.6(1)[b]
		1813.1(3)	1181.23(7)	4^+	3.4(4)[a]
		2429.49(22)	564.12(1)	2^+	0.85(11)[b]
2997.96(8)	3,4	1816.7(3)	1181.23(7)	4^+	2.6(5)[a]
3003.8(2)[d]		596.76(9)[e]	2407.12(9)	5^-	0.6(3)[a]
3017.4(4)[d]		734.03(9)[e]	2283.45(7)	6^+	1.6(2)[a]
3026.77(6)	2^+	468.81	2557.74(7)	2,3	0.6(4)[a]
		1074.90(10)	1951.68(5)	3^+	0.57(12)[b]

TABLE I. *(Continued.)*

E_x (keV)	I^π	E_γ	E_f	I_f^π	Int.
		1770.7(3)	1256.83(4)	2^+	1.5(3)[a]
		2462.5(21)	564.12(1)	2^+	0.34(7)[b]
3030.49(10)	6^+,5,4	1120.77(3)[e]	1909.50(5)	4^+	0.9(3)[a]
		1849.1(1)	1181.23(7)	4^+	4.3(3)
3046.8(2)[d]		1295.9(1)[e]	1750.91(9)	6^+	3.1(2)[a]
3052.1(5)[d]		644.6(12)[e]	2407.12(9)	5^-	0.9(3)[a]
		768.73(11)[e]	2283.45(7)	6^+	0.9(2)[a]
3074.07(12)	(8^-)	273.13(3)	2800.82(10)	7^-	0.75(24)[a]
3077.4(1)[d]		670.35(11)[e]	2407.12(9)	5^-	1.2(3)[a]
3099.4(2)[d]		429.64(3)[e]	2669.78(14)	8^+	1.6(3)[a]
3104.3(3)[d]		1194.8(2)[e]	1909.50(5)	4^+	1.0(3)[a]
3123.2(4)[d]		1372.4(2)[e]	1750.91(9)	6^+	1.4(3)[a]
3143.8(3)[d]		736.7(2)[e]	2407.12(9)	5^-	0.8(4)[a]
3157.4(3)[d]		874.0(3)[e]	2283.45(7)	6^+	0.7(3)[a]
3166.4(4)[d]		1415.5(4)[e]	1750.91(9)	6^+	2.0(3)[a]
3210.22(12)		1300.2(1)[e]	1909.50(5)	4^+	0.9(4)[a]
3210.9(3)[d]		297.40(4)[e]	2913.5(4)	(8^+)	1.8(2)[a]
3285.2(1)[d]		1375.1(3)[e]	1909.50(5)	4^+	1.7(3)[a]
3290.93	(10^+)	621.99(4)	2669.78(14)	8^+	0.7(2)[a]
3324.3(4)[d]		1573.4(4)[e]	1750.91(9)	6^+	3.5(2)[a]
3334.68(20)[d]		664.9(4)[e]	2669.78(14)	8^+	0.4(3)[a]
3366.2(2)[d]		1456.6(1)[e]	1909.50(5)	4^+	1.4(3)[a]
3382.0(3)[d]		712.22(4)[e]	2669.78(14)	8^+	0.71(15)[a]
3415.3(3)[d]		745.52(3)[e]	2669.78(14)	8^+	0.81(18)[a]
3626.2(3)[d]		957.1(3)[e]	2669.78(14)	8^+	0.5(3)[a]
3684.9(3)[d]		1015.9(3)[e]	2669.78(14)	8^+	0.7(4)[a]

[a]Evaluated from coincidence data.
[b]Not observed owing to low intensity or being out of energy range; intensity deduced using the branching ratio from Ref. [4].
[c]Not observed owing to low intensity or being out of energy range; intensity deduced using the branching ratio from ENSDF [5].
[d]New level.
[e]New γ-ray transition.

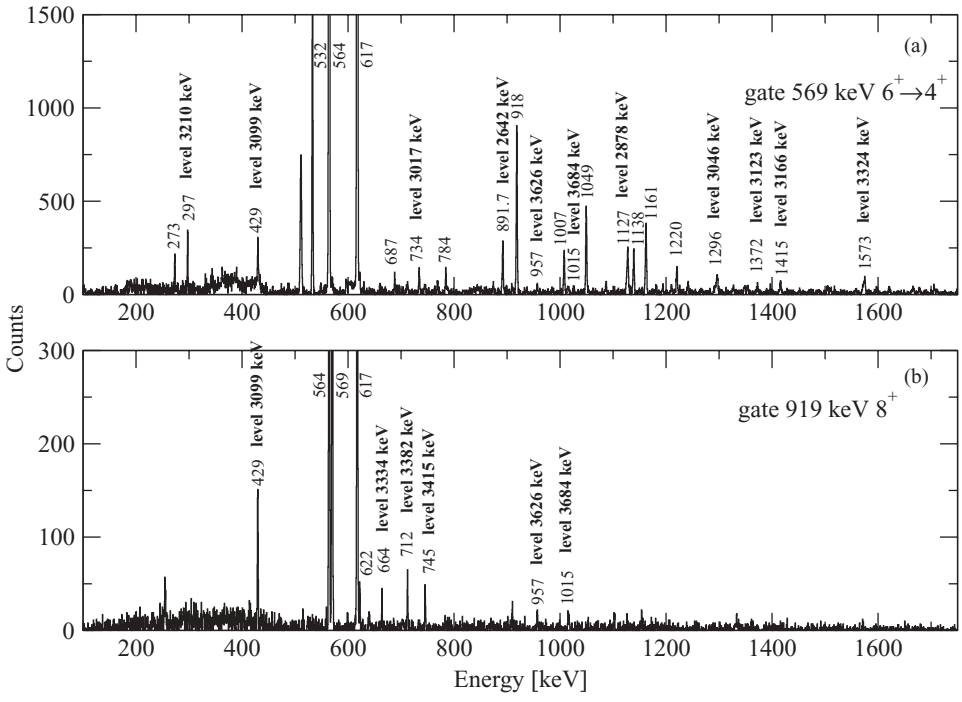

FIG. 1. $\gamma\gamma$ coincidence spectra obtained following the ^{119}Sn$(\alpha,n)^{122}$Te reaction at 15-MeV beam energy. γ-ray peaks are labeled with their energies. Peaks assigned to decays of some of the newly assigned levels (Table I) are also labeled with the level energy.

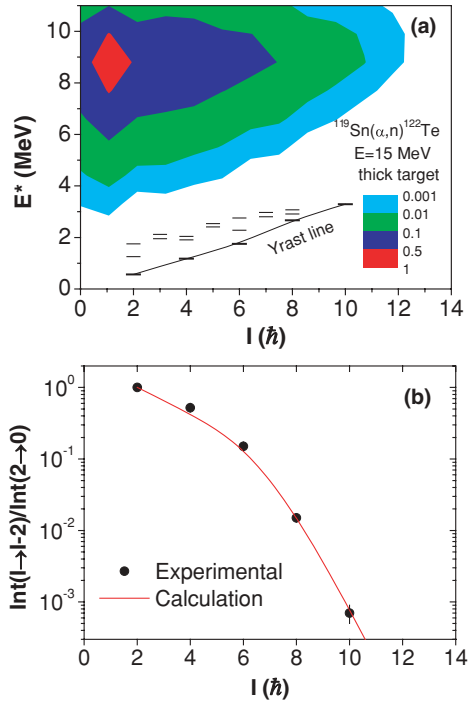

FIG. 2. (Color online) (a) Probability distribution of the population of entry states in the ^{119}Sn(α,n) reaction at 15.0 MeV, on a thick target. The yrast line and first few nonyrast states of each spin are shown. (b) Comparison between measured and calculated intensities for the yrast band $E2$ transitions.

In the following we analyze several features of the reaction ^{119}Sn(α,n)^{122}Te at 15 MeV. Figure 2(a) shows the distribution of the entry states in ^{122}Te (i.e., states populated after neutron emission), calculated with the COMPA program. The slowing-down of the α-particle beam in the thick target was taken into account. Both the yrast states and some of the known states above yrast are shown. It can be seen that the population probability has a maximum at low spins ($I = 1, 2\hbar$) and decreases sharply with spin. This distribution is drastically different from those corresponding to heavy-ion reactions: for example, in the neighboring nuclei ^{118}Te and ^{120}Xe, populated in the ^{109}Ag(^{13}C,$p3n$) reaction at 54 MeV [12] and ^{111}Cd(^{12}C,3n) reaction at 56 MeV [13], respectively, the distribution has a maximum located near spin $I = 10$–$12\hbar$. Each entry state is a starting point for side feeding γ-ray cascades, which are simulated with the program GAMMA. Because the maximum probability is situated at relatively high excitation energies (about 9 MeV), one can anticipate that the side feeding times will have important effects, depending on the location of the discrete level of interest. The need to take into account the side feeding delay time became obvious from the beginning of application of DSAM to the compound nuclear reactions. Some attempts to calculate the side feeding time distribution on the basis of the statistical theory [14] or of empirical methods taking into account both the statistical $E1$ [15] and the stretched $E2$ [16] transitions have been proposed. The simplest approach is to describe the side feeding delay by one single parameter, which is the effective lifetime τ_{sf} of a virtual level that feeds the level of interest, the value of τ_{sf} varying linearly with the energy of the investigated level [17]. Such an approach was used for a long time in the DSAM application for α-particle-induced reactions [18–24]. Later, this empirical method was modified so as to take into account the stretched side feeding cascades [7,12,13]. Similar empirical approaches work satisfactorily only if τ_{sf} is significantly shorter than both the level lifetime and the recoil stopping time but are hardly suitable for (α,n) reactions on medium-mass targets ($A \approx 100$). The only suitable approach is to include the simulation of the side feeding cascades from each entry state directly in the line-shape calculation. Here, the competition among statistical $E1$, $M1$, and $E2$ transitions, as well as stretched $E2$ and $M1$ transitions, defines the distribution of the side feeding times t_{sf}, that is, the times needed by these cascades to reach the destination level from the entry states. Simultaneously with t_{sf}, other features of the cascades, such as the multiplicity distribution and the distribution of the intensities along the yrast band, are calculated. A brief description of the side feeding model is given in Ref. [8], where a comparison of the experimental and calculated populations of the yrast band for the reaction ^{124}Sn(^{14}N,5n) reaction at 70 MeV was used for the determination of the side feeding model parameters, later used within the DSAM analysis. A similar method was used in the ^{122}Sn(^{10}B,4n) reaction for the investigation of chiral bands in ^{128}Cs [25]. In both these cases it turned out that the intensity and time distributions are mainly defined by features of the stretched $E2$ and $M1$ transitions, and depend only slightly on the statistical transitions. This approach was also used in the present case.

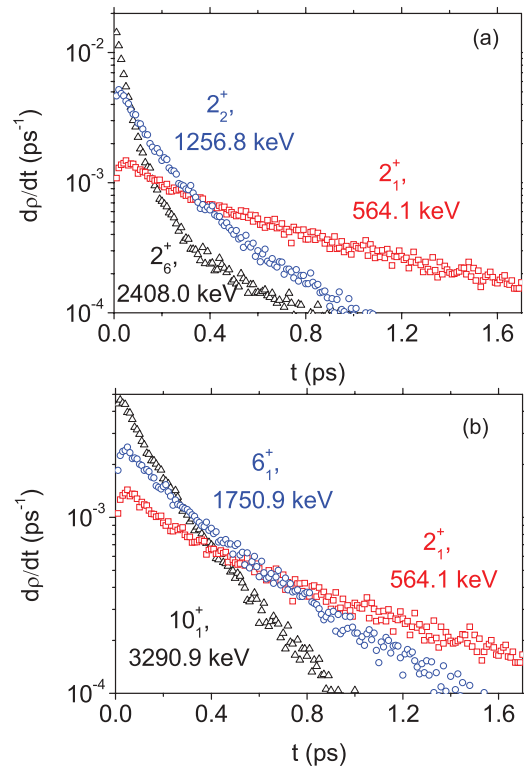

FIG. 3. (Color online) Examples of Monte Carlo calculated probability distributions of side feeding times for different excited states.

Figure 2(b) shows the experimental and calculated intensities of the $I \rightarrow I-2$ yrast transitions in ^{122}Te, normalized to the $2_1^+ \rightarrow 0_{gs}^+$ transition. It turned out that the good agreement shown in Fig. 2(b) is practically independent of the side feeding model parameters. This fact can be explained by the dominant role of the statistical (mainly $E1$) transitions in the side feeding pattern, which practically does not change the spin value of an entry state after the γ cascade. As a result, the calculated distribution mainly reflects the entry-state distribution, with Fig. 2 showing that the compound nucleus formation, as well as the neutron evaporation pattern calculated by COMPA, is confirmed by the experimental results. In this situation, only experimental data connected with the time evolution of side feeding cascades can be useful for the evaluation of statistical cascade parameters. In our case, very useful information was obtained from a comparison with absolute level lifetimes measured in the absence of side feeding, such as the measurements in Ref. [4] using the (n,n') reaction. As will be seen, this comparison allowed us to choose a value of $\sigma_0 = 273 \pm 50$ MeV^{-3} for the $E1$ giant resonance parameter.

Before presenting examples of DSAM analysis, the importance of proper calculation of side feeding times is stressed. Figure 3 shows examples for the distribution of the probability of a side feeding population for three different 2^+ states and for three states from the yrast line in ^{122}Te. It can be seen that these distributions differ from state to state, which emphasizes the necessity of proper calculation of the side feeding time for each state.

We compare our lifetimes with those from the $(n,n'\gamma)$ study [4] after fitting and fixing the value of σ_0. Actually, this fit depends on the stopping power used. In Ref. [4] nuclear stopping and scattering were described in the framework of the approach of Winterbon [26] and systematic errors related to the uncertainty of the stopping power were not taken into account (resulting, sometimes, in too small uncertainties).

Our nuclear stopping power parameters were evaluated experimentally for the close case of the stopping of I recoils into Ag [6,17] using the "semithick target" method [27,28]. The slowing-down process was approximated by the expression $d\rho/d\varepsilon = f_e k\sqrt{\varepsilon} + f_n\sqrt{\varepsilon}/(0.67 + 2.07\varepsilon)$, where ε and ρ are the energy and the range, respectively, expressed as Lidhard's units, k is the Lindhard electronic stopping power coefficient, and f_e and f_n are correction factors of the Lindhard cross sections, which were evaluated as $f_e = 1.27 \pm 0.07$ and $f_n = 0.77 \pm 0.07$. Therefore, the nuclear stopping power parameter differs from the standard one (the Lindhard value is $f_n = 1$, while for the Ziegler universal potential the new

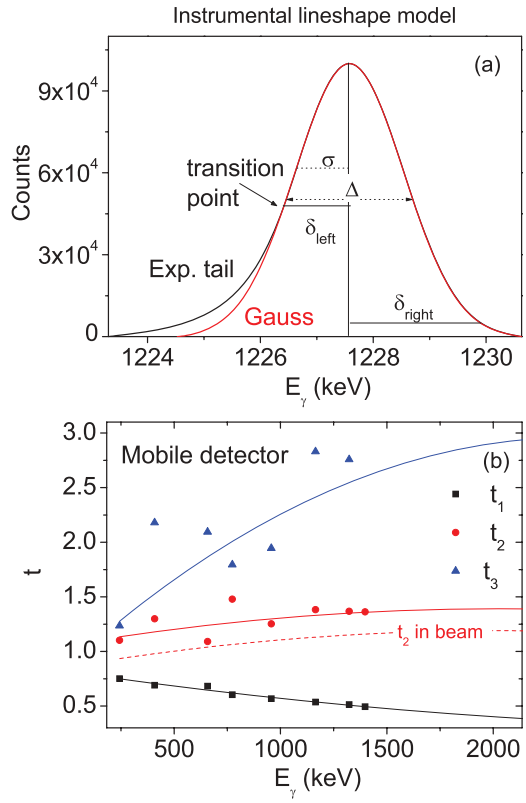

FIG. 4. (Color online) (a) Illustration of the parametrization of the detector response line (or instrumental line shape). (b) Polynomial fit of the parameters of the instrumental line shape as a function of energy (here, for the mobile detector of this experiment).

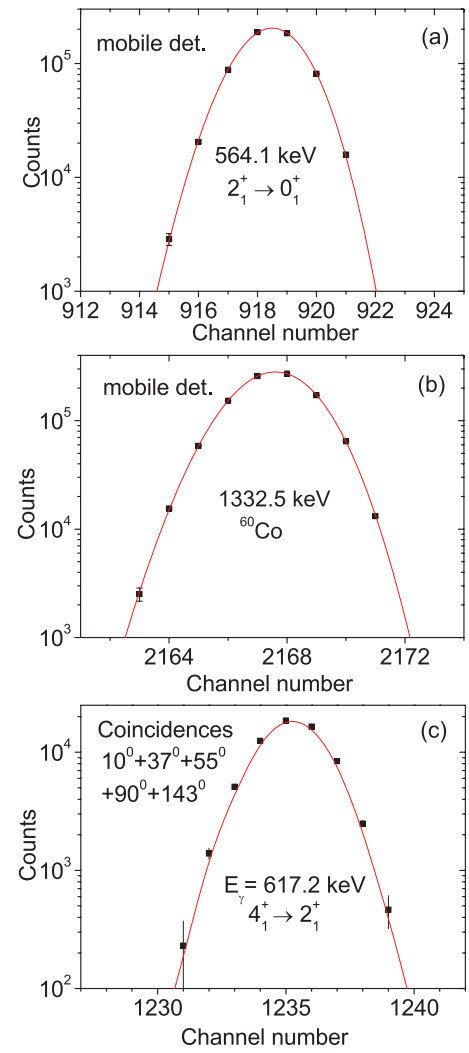

FIG. 5. (Color online) Illustration of the description of some experimental peaks by the employed instrumental line-shape function.

estimation is $f_n \approx 0.9$ [28]). Furthermore, the electronic stopping power component in the (α,n) reaction is not negligible and also influences the results of the determination of σ_0 and τ. Thus, in calculating the reduced transition probabilities $B(\sigma,\lambda)$ we take into account an additional error owing to uncertainties in the stopping powers. In our case the velocity is lower, therefore the nuclear stopping mechanism becomes dominant, with the main stopping power uncertainty of about 10% arising from this component. Because both the velocity range and the combination recoil nucleus-target are different, we adopted the slightly increased overall uncertainty of 15% in the stopping power.

TABLE II. Lifetimes determined for excited states in ^{122}Te by the present DSAM line-shape analysis. For levels followed by an asterisk, DSAM analysis was used to determine the value of the parameter σ_0 of the $E1$ transition strength function (see Sec. III D) by comparison with the lifetime values from Ref. [4]. Note that the final, adopted lifetime values are reported in Table III, after including an additional 15% error owing to the uncertainties in the stopping powers (as discussed in Sec. III B), which is not included in the lifetimes here.[a]

E_x (keV)	E_γ (keV)	τ (fs)	
		Present	Ref. [4]
1752.6*	1752.6	$1070^{+190}_{-140}{}^{b}$	1230^{+450}_{-260}
1909.5	1345.6	1400^{+130}_{-110}	1230^{+510}_{-280}
2099.2*	1535.4	380 ± 15^{b}	377^{+30}_{-27}
2283.5	1102.7	$210 \pm 15^{f,p}$	214^{+420}_{-102}
2310.7*	1747.1	575 ± 45^{f}	544^{+76}_{-64}
2407.1	1226.2	$340 \pm 30^{b,f,c}$	303^{+41}_{-32}
2408.0*	1844.4	$140 \pm 8^{b,f}$	137 ± 8
2448.5*	1267.3	$325^{+95}_{-65}{}^{c}$	341^{+51}_{-43}
2535.7	1354.4	500 ± 60^{b}	>680
2538.6	1357.3	$1150^{+850}_{-350}{}^{f}$	>1100
2600.8	1419.2	$1150^{+430}_{-220}{}^{b,f}$	1080^{+1790}_{-440}
2603.7	1422.4	$425^{+65}_{-40}{}^{b,f}$	–
2669.8	918.4	$230^{+70}_{-50}{}^{b,f,c}$	–
2679.4	2116.0	$650^{+150}_{-110}{}^{b,f}$	599^{+257}_{-142}
2758.8	1007.3	$>1000^{b,f}$	–
2800.8	1049.3	$660^{+110}_{-80}{}^{b,f}$	–
2810.0	1628.6	$320^{+27}_{-22}{}^{b,f}$	–
2816.7	1635.9	$1220^{+390}_{-230}{}^{b,f}$	903^{+1150}_{-340}
2878.3	1127.4	$580^{+120}_{-80}{}^{c}$	–
2913.5	1161.8	$630^{+140}_{-90}{}^{f}$	–
2930.7*	1750.5	$66^{+17}_{-14}{}^{b,f}$	60^{+8}_{-7}
3030.5*	1849.1	225^{+35}_{-30}	233^{+57}_{-41}
3166.4	1415.5	$125^{+35}_{-30}{}^{b,f}$	–
3324.3	1573.4	$630^{+260}_{-180}{}^{b,f}$	–

[a]*Used for the determination of σ_0. [b]From the "backward"-angle (143°) spectrum; [f]from the "forward"-angle (10° + 37° + 55°) spectra; [c]from coincidence spectra; [p]from the 90° spectrum.

The formulas used in the GAMMA program to calculate f_{E1} and σ_0 are outlined in Refs. [29] and [30]. The quantity f_{E1} may have large fluctuations with the mass number A [29,31]. Therefore, an indirect evaluation of σ_0, as discussed later, is rather important.

C. Analysis of instrumental line shapes

In the DSAM analysis of the Doppler broadened line shapes it is essential that the detector response (or the instrumental line shape) is accurately measured and evaluated as a function of the γ-ray energy. We determined this detector response function from spectra with radioactive sources using a dedicated code, SINGL. The parametrization of the response peak shape is illustrated in Fig. 4(a), as a Gaussian skewed with exponential tails on both sides of the peak. The Gaussian width σ (or t_1) and the decay constants of the two exponentials (t_2 and t_3), smoothly joined to the Gaussian on the left and right side, are model parameters, fitted to the experimental lines. After fitting the parameters for different γ rays of radioactive sources, the code produces a file with polynomial approximations for the energy dependence of the three parameters, which is used in the code SHAPE. Figure 4(b) shows, as an example, the parameters measured for the mobile detector. As a rule, the right side of the peak is very close to the Gaussian shape, which is reflected in the large values of the parameter t_3. Another point is that very often the instrumental shapes measured in-beam differ slightly from those measured off-beam, therefore a correction of the parameters must be done using lines from the in-beam spectra. In our case, we used the lines from a ^{60}Co source placed in the vicinity of the reaction chamber. Several clean and strong lines from ^{122}Te could also be used. The result of this correction is shown by the dashed line in Fig. 4(b). The small difference between the in-beam and the off-beam cases is still important for analyses of cases with a small Doppler effect. Figure 5 illustrates the excellent accuracy of the instrumental line-shape description.

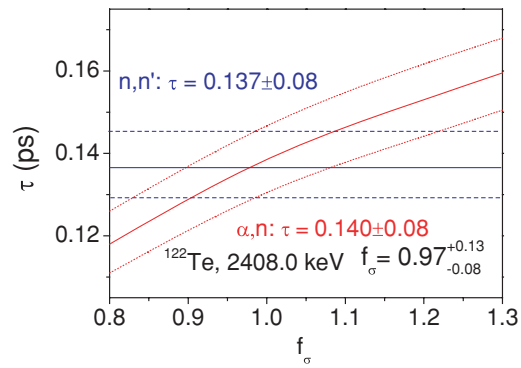

FIG. 6. (Color online) Influence of f_σ on the extracted lifetime. This graph refers to the transition 1844.4 keV (2408.0-keV level) and shows that the result of the present analysis coincides with that of the (n,n') reaction [4] for a value of f_σ that is practically 1.

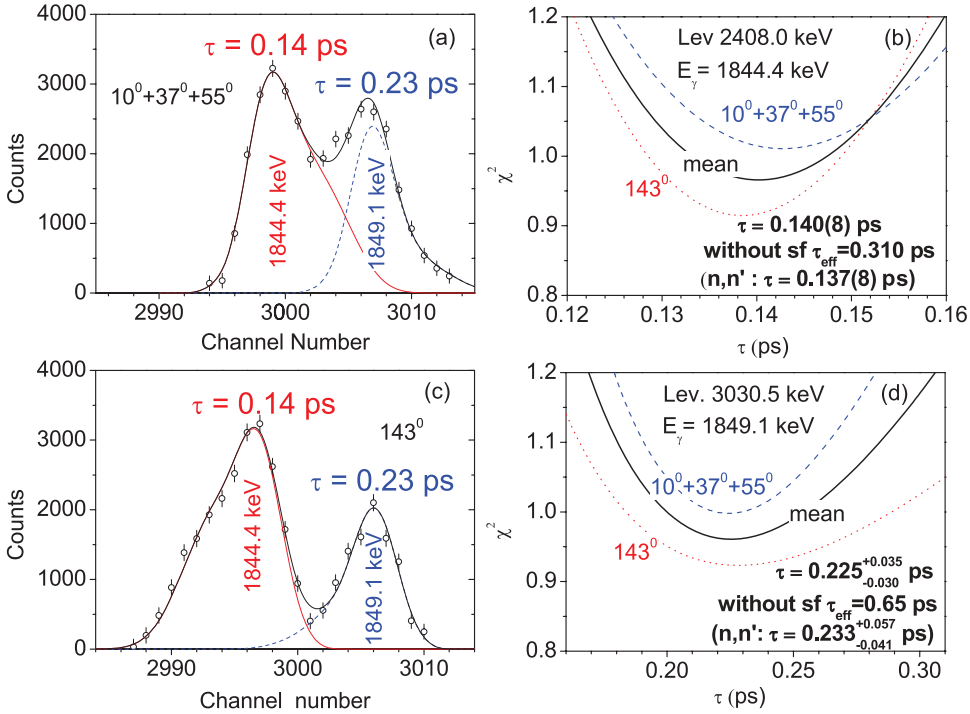

FIG. 7. (Color online) DSAM line-shape analysis of two transition γ rays, 1844.4 and 1849.1 keV, de-exciting the levels at 2408.0 and 3030.5 keV, respectively (energies of both γ rays and de-exciting levels are indicated). (a, c) Analysis performed at the forward and backward angles, respectively, from singles spectra; (b, d) χ^2 analysis of the fit providing the extracted lifetime (indicated). Lifetimes measured with the (n,n') reaction [4] are also shown for comparison. The line-shape analysis was performed with a value $f_\sigma = 1$. See discussion in Sec. III D for other details.

D. Lifetime analysis for side feeding parameter evaluation

The side feeding model takes into account $E1$, $M1$, and $E2$ statistical, as well as stretched $E2$ and $M1$, transitions. As discussed previously, in the case of (α,n) reactions the statistical $E1$ transition strength f_{E1} plays the dominant role. In the programs COMPA and GAMMA the calculation of this strength function is based on the approximation described in Refs. [29] and [30]. For nearly spherical nuclei with $A > 50$,

$$f_{E1} = 8.7 \times 10^{-8} \sigma_0 E_\gamma^2 \Gamma_0^2 / \left[\left(E_\gamma^2 - E_0^2 \right)^2 + E_\gamma^2 \Gamma_0^2 \right],$$

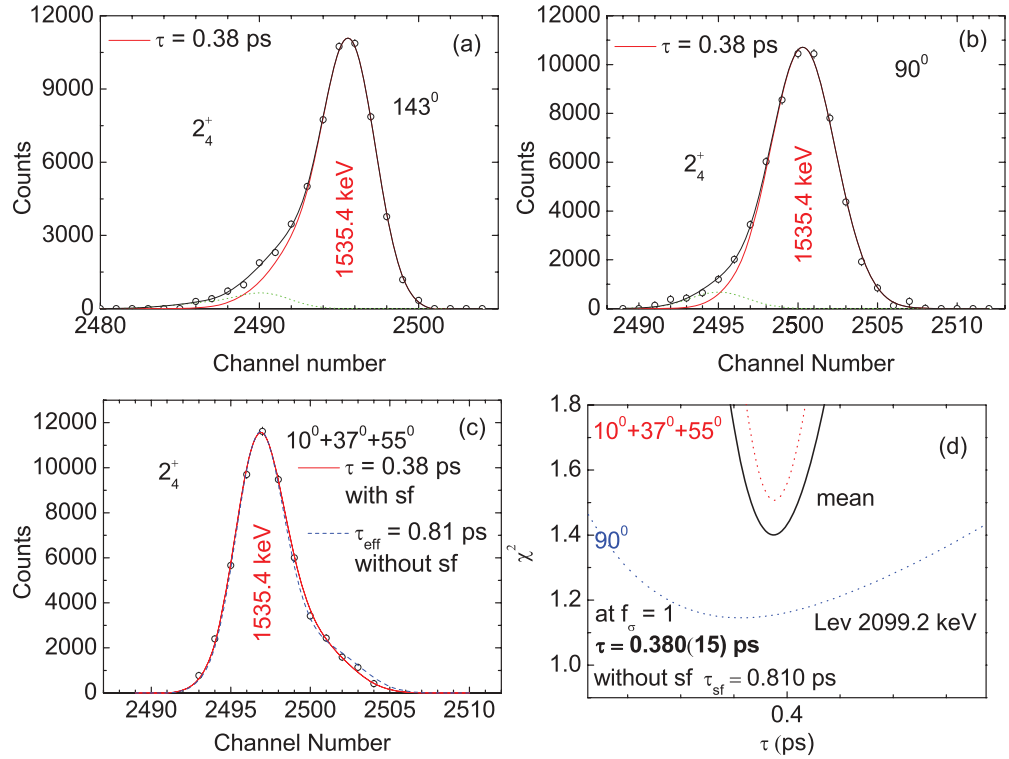

FIG. 8. (Color online) Similar to Fig. 7, but for the line-shape analysis of the 1535.4 keV-line (from the 2099.2-keV state) from the singles spectra at the indicated angles. A small contaminant peak of lower energy had to be considered.

where $E_0 = 50/A^{0.24}$, $\Gamma_0 = 0.3E_0$, and $\sigma_0 = \sigma_0^{\rm DB} = 10.6A/\Gamma_0 = 0.707 \times A^{1.24}$. For ^{122}Te this corresponds to a value of $\sigma_0^{\rm DB} = 273$ MeV^{-1}. A similar result is obtained from the experimental systematic of f_{E1} [29], $\sigma_0 = \sigma^{\rm sys} = 0.166 \times A^{1.54}$, which provides, for ^{122}Te, a value of $\sigma^{\rm sys} = 271$ MeV^{-1}. Nevertheless, it is known that estimated f_{E1} values show considerable fluctuations with mass number, and in cases where it is possible, comparison with experimental data shows deviations of up to a factor of 2. Thus, an indirect evaluation of σ_0, as performed in this work, is important. To characterize these fluctuations, we introduce the correction factor f_σ, $\sigma_0 = f_\sigma \sigma_0^{\rm DB}$, and evaluate f_σ on the basis of a comparison of lifetimes obtained in the present analysis with other independent determinations. In the case of ^{122}Te, many lifetimes were determined by the DSAM method with the (n,n') reaction [4], but other determinations with alternative methods are scarce (for the 2_1^+ and 2_2^+ states only, there are also determinations from Coulomb excitation, but in the first case the lifetime is outside the DSAM range, while in the latter the accuracy is only about 25% [5]). Therefore, we have compared our results with those for the the (n,n') reaction [4], which, although measured at lower recoil velocities, are independent of the side and cascade feedings.

Table II lists the levels of ^{122}Te for which lifetimes were deduced from the DSAM line-shape analysis of this work; for some of these levels, the lifetimes from Ref. [4] are also given. The levels followed by an asterisk are those for which σ_0 was adjusted so as to obtain a lifetime value comparable to that of the (n,n') reaction determination. All these levels have only direct feeding in our reaction. Figure 6 illustrates the influence of f_σ on the line-shape analysis, and also the comparison with the lifetime measured in the (n,n') reaction, for the level at $E_x = 2408.0$ keV. The intersection of the curve for the resulting lifetime τ as a function of f_σ with the value $\tau = 137 \pm 80$ fs determined in the (n,n') reaction gives a value $f_\sigma = 0.97$, with an error of about 10%. For the other six levels followed by an asterisk in Table II, which have different lifetime, spin, and energy position with respect to the yrast line, we get f_σ values between 0.95 and 1.08, with somewhat larger uncertainties. The resulting average value is $f_\sigma = 1.0 \pm 0.1$. Consequently, we have adopted the value $f_\sigma = 1$, which means $\sigma_0 = 273$ MeV^{-1}. The lifetimes listed in Table II correspond to this average value of σ_0. We emphasize

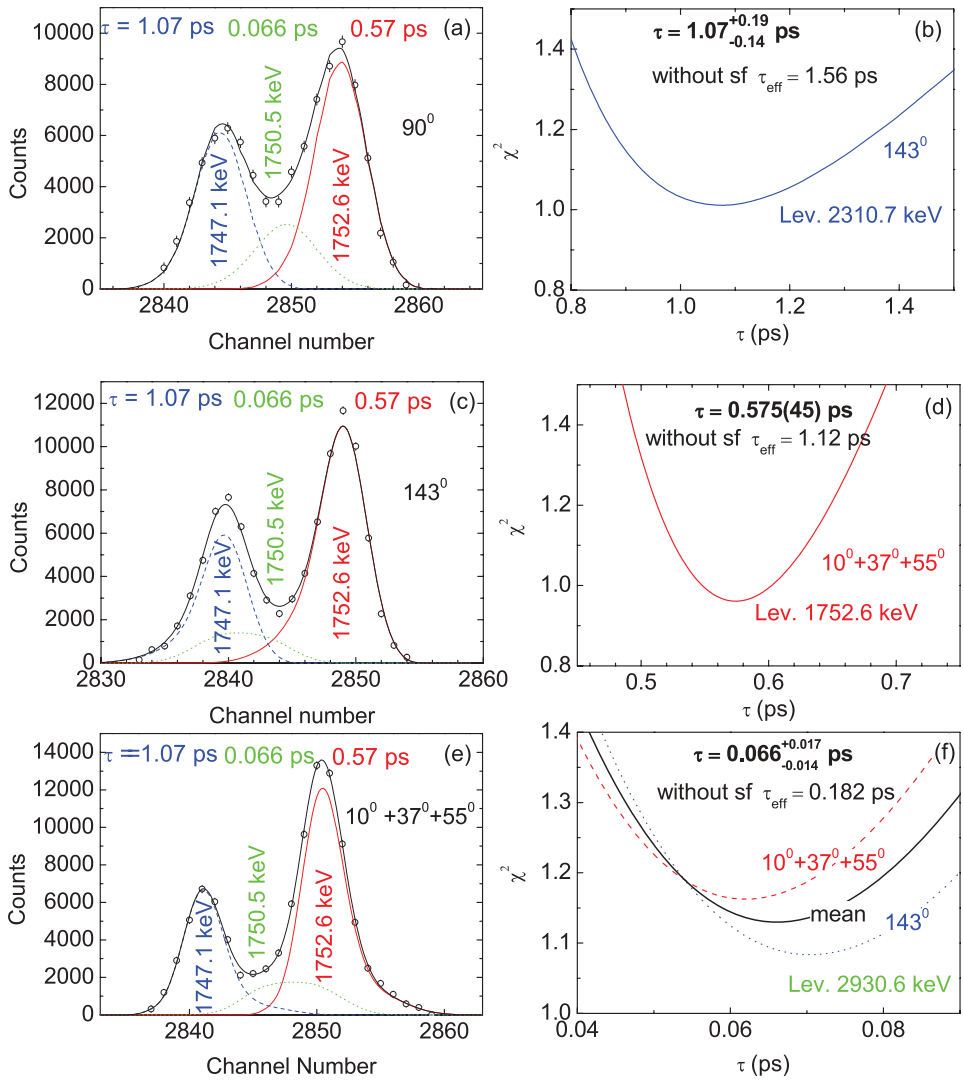

FIG. 9. (Color online) Similar to Fig. 7, for three overlapping transitions, 1747.1, 1750.5, and 1752.6 keV (from the decay of the 2310.7, 2930.7, and 1752.6 keV states, respectively), from singles spectra. The influence of the side feeding times is emphasized in each panel with the χ^2 analysis.

that the f_σ value depends on the stopping powers employed, and therefore its error should also include the uncertainties in the stopping power. Taking a 15% uncertainty in stopping powers, the uncertainty in σ_0 is estimated to be about 18%, therefore $\sigma_0 = 273 \pm 50$ MeV^{-1}, as stated in Sec. III B. The next figures show line-shape analyses made with this value and the resulting lifetimes.

Figure 7 shows the line-shape analysis of two γ rays: the 1844.4-keV transition from $E_x = 2408.0$ keV (the 2_7^+ state; Table I), and 1849.1 keV, which is a transition from the $E_x = 3030.5$ keV state ($J^\pi = 6^+, 5, 4$; Table I). Owing to the short lifetimes and high γ-ray energy, the Doppler broadened line shapes are quite visible for these lines at both backward and forward angles, especially that of the 1844.4-keV transition. The lifetimes of both these states were measured in the (n,n') reaction [4] and constitute a good test for our DSAM analysis. For both these levels we did not find cascade feeding (from known discrete levels), therefore the line-shape analysis is a good example of the influence of the side feeding times. As shown in Fig. 7, at the backward angle the line shape of the 1844.4-keV transition is slightly affected by that of the 1849.1-keV line. Without taking into account the side feeding correction, we get effective lifetimes of 310 and 650 fs for the levels at 2408.0 and 3030.5 keV, respectively. If the side feeding is calculated as described previously, then both the backward and the forward angle analyses provide lifetimes of 140 ± 8 and 225^{+35}_{-30} fs, in excellent agreement with the values 137 ± 8 and 233^{+57}_{-41} fs, respectively, from the (n,n') experiment [4]. This is a good validation for the choice of the σ_0 value as discussed before.

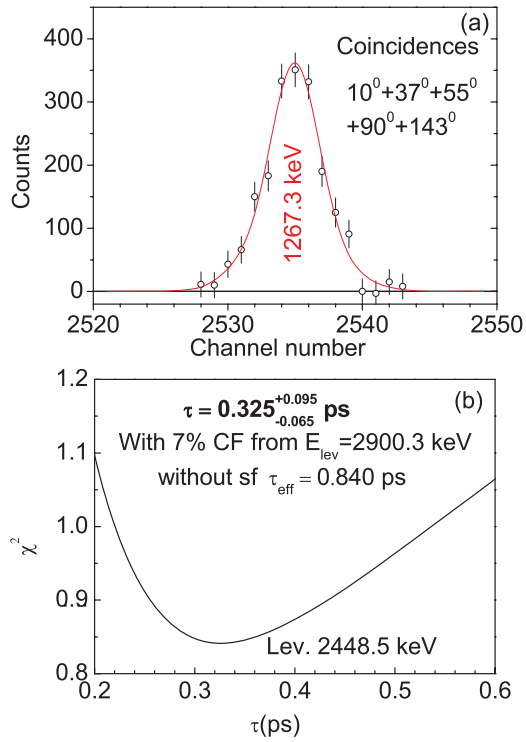

FIG. 10. (Color online) Line-shape analysis of the 1267.3-keV transition from the 2448.5-keV level, from a summed coincidence spectrum.

Figure 8 shows the analysis of the 1535.4-keV γ ray that decays the $E_x = 2099.2$ keV (2_4^+) state. At 143° and 90° the line shape is slightly contaminated by an impurity line, but in the forward direction it is clean. Analyses at different angles provide the value $\tau = 380 \pm 15$ fs for this state, in very good agreement with the value from the (n,n') experiment, 377^{+30}_{-27} fs. Again, the influence of the side feeding time is very important: without considering the side feeding time, one gets an effective lifetime of 810 fs.

Figure 9 shows the analysis of a more complex situation, with three overlapping γ rays—1752.6, 1747.1, and 1750.5 keV—representing the decay of the levels at 1752.6 keV (2_3^+), 2310.7 keV (2_6^+), and 2930.7 keV ($I = 4, 5$), respectively. The lifetimes obtained for these levels cover the range from 60 to about 1100 fs and agree quite well with those from the (n,n') experiment [4] (see Table II). In each case, the important influence of the side feeding times is emphasized in Figs. 9(b), 9(d), and 9(f).

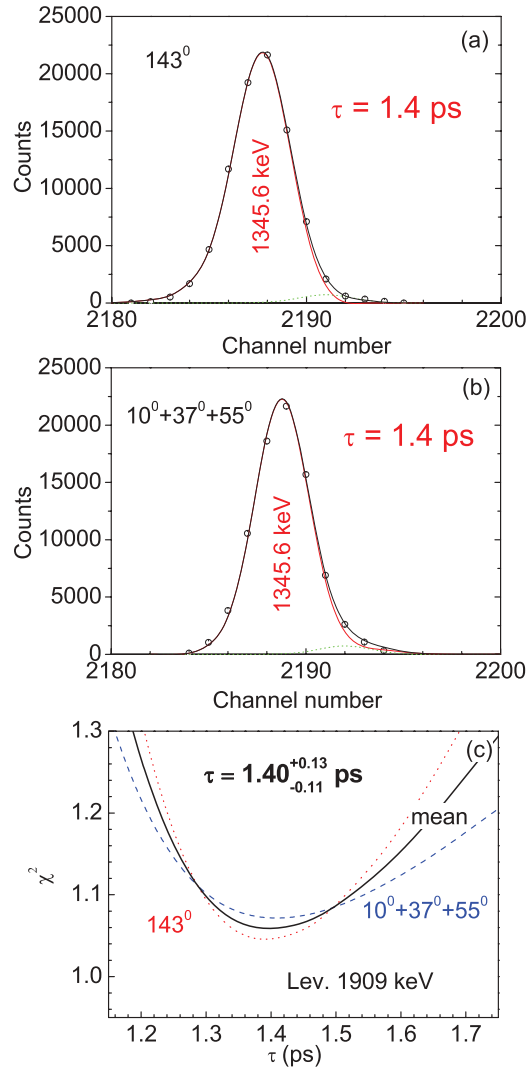

FIG. 11. (Color online) DSAM analysis of the line shape of the 1345.6-keV transition from the 1909.5-keV state. Both side feeding and cascade feeding (see discussion in Sec. III E) were considered in this analysis.

TABLE III. Lifetime and electromagnetic transition rate information for excited states of ^{122}Te, as deduced from the present experiment. The information is for the same levels that are listed in Table II. The τ_{corr} lifetime values in the third column contain a 15% uncertainty in the stopping power (see discussion in Sec. III F and Fig. 23). Transition rates $B(\sigma,\lambda)$ were evaluated with the Monte Carlo procedure described in Sec. III F, taking into account asymmetrical errors in lifetime and mixing ratio, as well as the uncertainty in the stopping power. For states with unknown spin three B values are listed, corresponding to the indicated pure multipolarity.

E_x (keV)	τ (ps)	τ_{corr} (ps)	E_γ (keV)	$I_i^\pi \rightarrow I_f^\pi$	I_γ	δ[a]	$\sigma\lambda$	B($\sigma\lambda$) (W.u.)	
								B	B_{median}
1909	$1.40^{+0.13}_{-0.11}$[b]	$1.39^{+0.24}_{-0.14}$	653	$4_2^+ \rightarrow 2_2^+$	7.4(3)	–	$E2$	14^{+3}_{-2}	15
			728	$4_2^+ \rightarrow 4_1^+$	35.1(7)	$4.46^{+0.72}_{-0.56}$	$M1$	$1.3^{+0.6}_{-0.3} \times 10^{-3}$	1.4×10^{-3}
							$E2$	38^{+8}_{-5}	40
			1345	$4_2^+ \rightarrow 2_1^+$	23.5(6)	–	$E2$	$1.25^{+0.28}_{-0.17}$	1.30
2283	0.210 ± 0.015[b]	$0.207^{+0.034}_{-0.030}$	533	$6_2^+ \rightarrow 6_1^+$	19.6(5)	$0.19^{+0.54}_{-0.25}$	$M1$	$0.42^{+0.11}_{-0.10}$	0.42
							$E2$	<300	170
			1103	$6_2^+ \rightarrow 4_1^+$	17.5(6)	–	$E2$	30^{+9}_{-5}	32
2407	0.325 ± 0.025[b]	$0.322^{+0.057}_{-0.052}$	1226	$5_1^- \rightarrow 4_1^+$	36.5(11)	–	$E1$	$6.4^{+1.3}_{-0.9} \times 10^{-4}$	6.6×10^{-4}
2536	0.50 ± 0.06[c]	$0.49^{+0.10}_{-0.09}$	1354	$5_1^{(+)} \rightarrow 4_1^+$	14.2(6)	$-1.01^{+0.27}_{-0.39}$	$M1$	$9.2^{+0.4}_{-0.2} \times 10^{-3}$	9.9×10^{-3}
							$E2$	$4.2^{+1.4}_{-1.1}$	4.4
			784	$5_1^{(+)} \rightarrow 6_1^+$	1.4(3)	–	$M1$	$9.9^{+4.5}_{-2.6} \times 10^{-3}$	1.10×10^{-2}
			626	$5_1^{(+)} \rightarrow 4_2^+$	1.5(2)	–	$M1$	$2.10^{+0.86}_{-0.45} \times 10^{-2}$	2.30×10^{-2}
2539	$1.15^{+0.85}_{-0.35}$[c]	$1.22^{+0.83}_{-0.42}$	587	$4_1^{(-)} \rightarrow 3_1^+$	12.7(6)	–	$E1$	$6.9^{+5.9}_{-1.8} \times 10^{-4}$	9.1×10^{-4}
			629	$4_1^{(-)} \rightarrow 4_2^+$	1.9(3)	–	$E1$	$8.6^{+7.4}_{-2.5} \times 10^{-5}$	1.1×10^{-4}
			1357	$4_1^{(-)} \rightarrow 4_1^+$	4.1(3)	–	$E1$	$1.8^{+1.6}_{-0.5} \times 10^{-5}$	2.4×10^{-5}
2601	$1.15^{+0.43}_{-0.22}$[b]	$1.17^{+0.46}_{-0.28}$	1419	$3_2^+ \rightarrow 4_1^+$	5.1(2)	2.0 ± 1.5	$M1$	$5^{+19}_{-2} \times 10^{-4}$	13×10^{-4}
							$E2$	$1.35^{+0.68}_{-0.65}$	1.38
			2036	$3_2^+ \rightarrow 2_1^+$	2.5(1)[a]	$-0.83^{+0.24}_{-0.29}$	$M1$	$4.6^{+3.6}_{-1.5} \times 10^{-4}$	5.7×10^{-4}
							$E2$	$5.7^{+4.9}_{-2.3} \times 10^{-2}$	6.8×10^{-2}
2604	$0.425^{+0.065}_{-0.040}$[c]	$0.430^{+0.092}_{-0.076}$	1422	$4_5^+ \rightarrow 4_1^+$	6.5(2)	$0.78^{+0.27}_{-0.69}$	$M1$	$1.77^{+0.65}_{-0.43} \times 10^{-2}$	1.88×10^{-2}
							$E2$	<3	2
2670	$0.23^{+0.06}_{-0.04}$[c]	$0.23^{+0.07}_{-0.05}$	918	$8_1^+ \rightarrow 6_1^+$	15.2(5)[b]	–	$E2$	134^{+46}_{-26}	145
2679	$0.635^{+0.125}_{-0.075}$[d]	$0.642^{+0.160}_{-0.119}$	1422	$4_7^+ \rightarrow 2_2^+$	1.5(3)[b]	–	$E2$	$1.62^{+0.53}_{-0.36}$	1.68
			2116	$4_7^+ \rightarrow 2_1^+$	3.6(1)[b]	–	$E2$	$0.54^{+0.15}_{-0.09}$	0.57
2758	$0.193^{+0.024}_{-0.019}$[a]	$0.192^{+0.039}_{-0.034}$	717	$5_1^{(+)} \rightarrow 4_3^+$	0.3(2)[c]	$3.1^{+3.5}_{-0.8}$	$M1$	$3^{+12}_{-2} \times 10^{-4}$	7×10^{-4}
							$E2$	23^{+18}_{-13}	25
			1577	$5_1^{(+)} \rightarrow 4_1^+$	6.7(6)	$0.51^{+0.12}_{-0.09}$	$M1$	$2.9^{+0.7}_{-0.6} \times 10^{-2}$	3.0×10^{-2}
							$E2$	$2.3^{+1.0}_{-0.6}$	2.5
2759	>1000[c]	>1000	351	$6_1^- \rightarrow 5_1^-$	7.2(4)	$-0.32^{+0.10}_{-0.08}$	$M1$	<0.1	5×10^{-2}
			1007	$6_1^- \rightarrow 6_1^+$	3.5(4)	–	$E2$	<60	30
2801	$0.66^{+0.11}_{-0.08}$[c]	$0.66^{+0.15}_{-0.13}$	393	$7_1^- \rightarrow 5_1^-$	0.5(1)[e]	–	$E2$	147^{+54}_{-35}	155
			1049	$7_1^- \rightarrow 6_1^+$	10.8(6)	–	$E1$	$4.6^{+1.2}_{-0.7} \times 10^{-4}$	4.8×10^{-4}
2810	$0.320^{+0.027}_{-0.022}$[c]	$0.318^{+0.0.056}_{-0.050}$	1629	$4^+, 3 \rightarrow 4_1^+$	3.5(5)	$0.03^{+0.22}_{-0.12}$	$M1$	$1.94^{+0.40}_{-0.27} \times 10^{-2}$	2.01×10^{-2}
							$E2$	<0.1	9×10^{-2}
			2245	$4^+, 3 \rightarrow 2_1^+$	0.31(3)[a]	–	$E2$	$9.5^{+3.0}_{-1.9} \times 10^{-2}$	9.9×10^{-2}
2817	$1.22^{+0.39}_{-0.23}$[b]	$1.23^{+0.42}_{-0.29}$	907	$4^+, 5^+ \rightarrow 4_3^+$	1.1(2)	$0.19^{+0.37}_{-0.28}$	$M1$	$4.9^{+2.6}_{-1.4} \times 10^{-3}$	5.4×10^{-3}
							$E2$	<0.9	0.4
			1636	$4^+, 5^+ \rightarrow 4_2^+$	4.6(5)	$0.47^{+0.13}_{-0.07}$	$M1$	$3.2^{+1.3}_{-0.7} \times 10^{-3}$	3.5×10^{-3}
							$E2$	$0.21^{+0.13}_{-0.06}$	0.24
2878	$0.58^{+0.12}_{-0.08}$[c]	$0.58^{+0.15}_{-0.12}$	1127	$\rightarrow 6_1^+$	7.0(4)	–	$M1$	$3.5^{+0.9}_{-0.7} \times 10^{-2}$	3.7×10^{-2}

TABLE III. *(Continued.)*

E_x (keV)	τ (ps)	τ_{corr} (ps)	E_γ (keV)	$I_i^\pi \rightarrow I_f^\pi$	I_γ	δ[a]	$\sigma\lambda$	B($\sigma\lambda$) (W.u.)	
								B	B_{median}
						–	$E2$	20^{+6}_{-4}	21
						–	$E1$	$4.3^{+1.3}_{-0.8} \times 10^{-4}$	4.6×10^{-4}
2913	$0.63^{+0.14}_{-0.09}$[c]	$0.63^{+0.17}_{-0.13}$	629	$8_2^+ \rightarrow 6_2^+$	0.3 ± 0.2[c]	–	$E2$	11^{+9}_{-6}	13
			1162	$8_2^+ \rightarrow 6_1^+$	8.2 ± 0.4	–	$E2$	15^{+5}_{-3}	16
3166	$0.125^{+0.035}_{-0.030}$[c]	$0.122^{+0.040}_{-0.036}$	1415	$\rightarrow 6_1^+$	2.0(3)	–	$M1$	$7.9^{+3.5}_{-1.6} \times 10^{-2}$	8.8×10^{-2}
						–	$E2$	28^{+13}_{-6}	32
						–	$E1$	$1.0^{+0.4}_{-0.2} \times 10^{-3}$	1.1×10^{-3}
3324	$0.63^{+0.26}_{-0.18}$[c]	$0.61^{+0.29}_{-0.19}$	1573	$\rightarrow 6_1^+$	3.5(2)	–	$M1$	$1.03^{+0.59}_{-0.25} \times 10^{-2}$	1.21×10^{-2}
						–	$E2$	$3.0^{+1.8}_{-0.7}$	3.5
						–	$E1$	$1.29^{+0.74}_{-0.31} \times 10^{-4}$	1.51×10^{-4}

[a]From Ref. [4].
[b]Revised value.
[c]New value.
[d]Adopted from this work and Ref. [4].
[e]From ENSDF [5].

The last example is given in Fig. 10, with the analysis of the 1267.3-keV transition from the 2448.5-keV (4_4^+) level. In the singles spectra this line is mixed up in a complex multiplet, so that we present an analysis of a clean coincidence spectrum summed over all measured angles, which provides a τ value in good agreement with the (n,n') data. Both the side feeding and the feeding from the 2900.3 keV level were taken into consideration in the analysis.

E. New and revised lifetimes

The level lifetimes in ^{122}Te measured in this work are reportted in Table II, in comparison with those from Ref. [4]. As mentioned in the previous section, a portion of these determinations (the levels followed by an asterisk) has been used for the determination of σ_0. The other determined lifetimes roughly fall into three categories: (i) newly determined values, (ii) revised values (if the error of our determination was considerably smaller than that in Ref. [4]), and (iii) values determined with an error comparable to that in Ref. [4]. In the latter case we adopted a τ value that is the weighted average of the two determinations (see Table III). The DSAM analysis of the line shapes took into account the side feeding times (as explained before), as well as the cascade feedings (i.e., the feeding from higher known discrete levels). In some

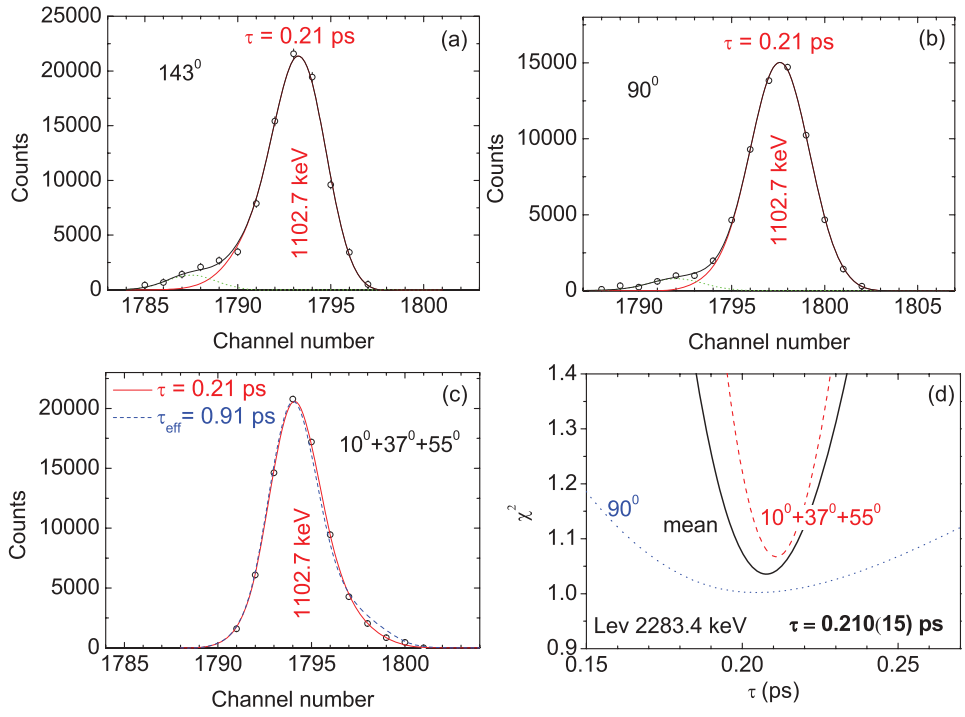

FIG. 12. (Color online) Same as Fig. 11 but for the line shape of the 1102.7-keV transition from the 2283.5-keV state.

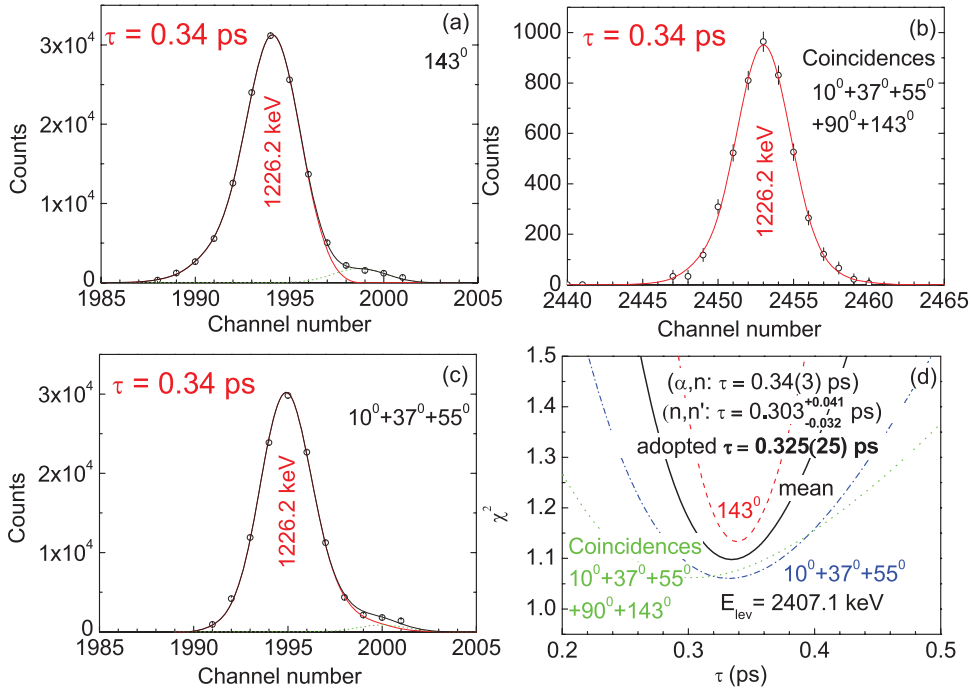

FIG. 13. (Color online) Same as Fig. 11, for the 1226.2-keV line from the 2407.1-keV level. The small contamination from the singles spectra (a, c) disappeared in the coincidence spectrum (b). The lifetime measured with the (n,n') reaction [4] is also shown for comparison (d).

cases, the lifetimes of the discrete feeding levels were known. When the lifetime was not known, it was assumed to be of the order of 1 ps or higher, therefore the cascade feeding contributes only in the stopped peak. This assumption appears to be justified because in many cases the analyzed level is fed by γ rays with a relatively low energy. We proceed here to a presentation of the DSAM analysis of all these levels, roughly in the order of their increasing excitation energy.

1. The 1909.5-keV, 4_2^+ state

The lifetime of this state was deduced from the line-shape analysis of the 1345.6-keV transition at both forward and backward angles, taking into account a small contamination line [Figs. 11(a) and 11(b)]. Figure 11(c) presents the χ^2 analysis. The lifetime was too large for the low-recoil (n,n') experiment, therefore it was determined with a large error in Ref. [4], while the error in our case is considerably smaller. In this analysis, besides the side feeding, cascade feeding

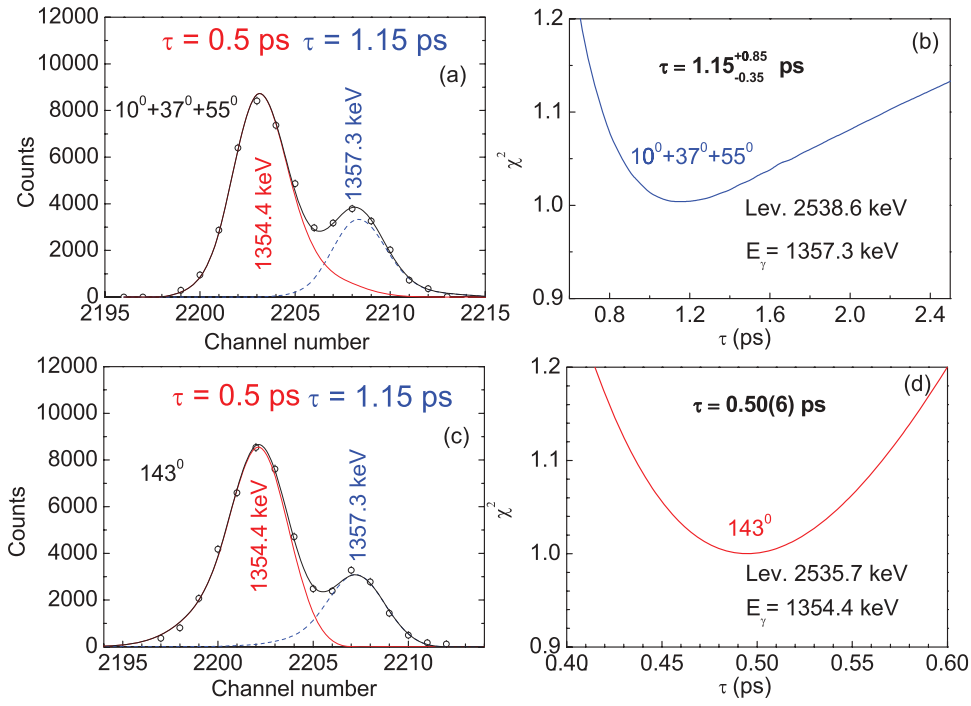

FIG. 14. (Color online) Same as Fig. 11, for the 1354.4- and 1357.3-keV lines from the levels at 2535.7 and 2538.6 keV, respectively.

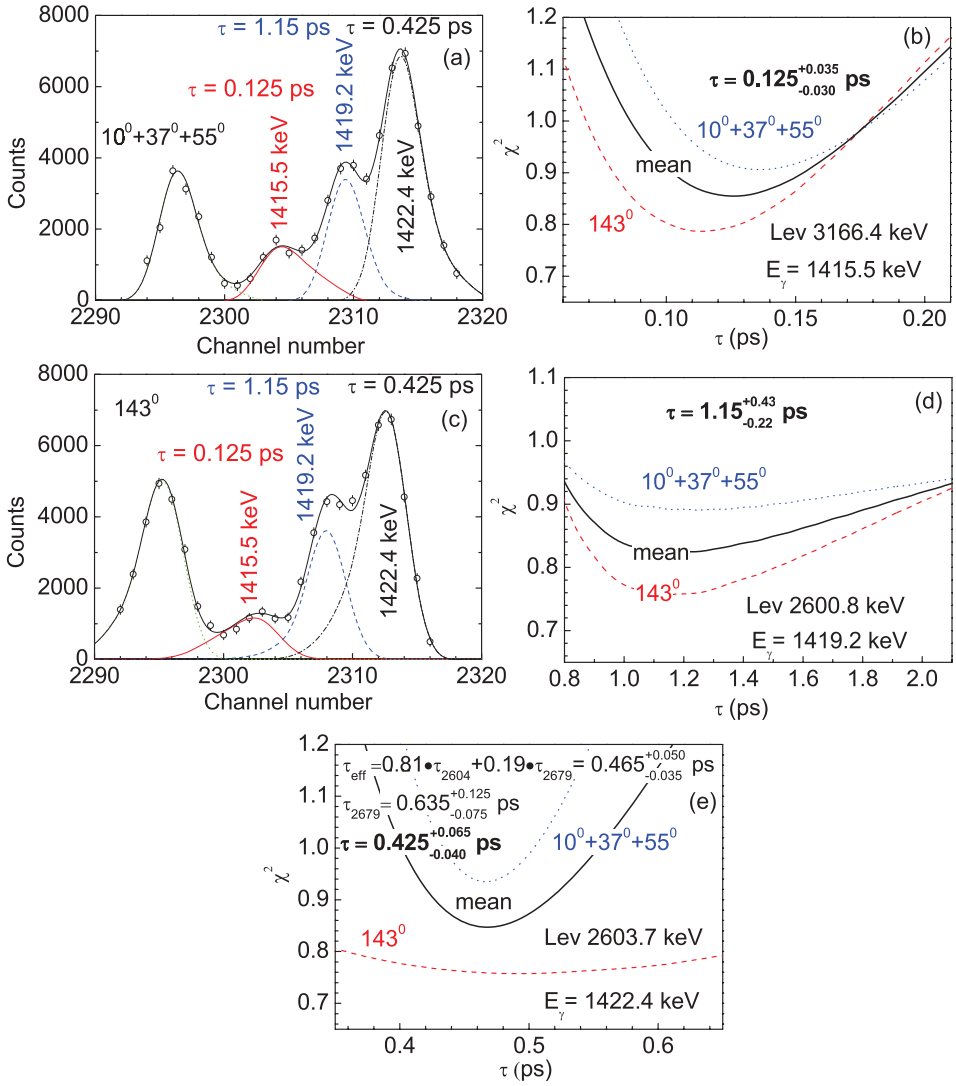

FIG. 15. (Color online) Same as Fig. 11 for three lines, 1415.5, 1419.2, and 1422.4 keV, from the decay of the levels at 3166.4, 2600.8, and 2603.7 keV, respectively. Note that the 1422.4-keV line has a contribution from the 2679.4-keV level, for which the lifetime is known from Ref. [4]. See discussion in Sec. III F.

summing up to 22% from the levels at 2448.5, 2535.7, 2538.6, 2642.8, 2816.7, 2960.7, 3104.3, 3210.2, 3285.2, and 3366.2 keV (Table I) was taken into consideration. Without side and cascade feeding accounted for, the extracted "effective" lifetime is $\tau_{\text{eff}} = 5.4$ ps; with side feeding taken into account, this decreases to $\tau = 1.91$ ps; and, finally, with cascade feeding included, one gets $\tau = 1.40^{+0.13}_{-0.11}$ ps.

2. *The 2283.5-keV,* 6_2^+ *state*

Its 1102.7 keV de-exciting γ ray is slightly disturbed by a small contamination at both 143° and 90°, while at the forward angles its Doppler tail is clean (Fig. 12). The forward and 90° angles were used to extract its lifetime. The level is 11% fed by the higher levels at 2889.7, 2913.5, 2971.9, 3017.4, 3052.1, and 3157.4 keV. The effective lifetime shown by this level is 0.91 ps; with the side feeding correction, it decreases to 0.24 ps; and it is further reduced to 0.21 ps upon also taking into account the cascade feeding. One can see that at the forward angles the line shape calculated with the effective lifetime does not describe the experimental points well.

3. *The 2407.1-keV,* 5_1^- *state*

Its 1226.2-keV line is slightly disturbed by a weak contamination line with a higher energy (Fig. 13). Seen in coincidence, the line is clean [Fig. 13(b)] and has enough statistics for the analysis. All three spectra presented in Fig. 13(b) were used to extract the lifetime. The effective lifetime is 0.61 ps. In the analysis, feeding from the higher states 2758.8, 2800.8, 2960.7, 2975.4, 3003.8, 3052.1, 3077.4, and 3143.8 keV levels resulted in a final value of 340 ± 30 fs, which has an error similar to that of, and is in good agreement with, the value reported in Ref. [4], 303^{+41}_{-32} fs; therefore we finally adopted the value $\tau = 325 \pm 25$ fs, which was used for determination of the corresponding $B(E1)$ value (Table III).

4. *The 2535.7-keV,* $\mathbf{I = 5}$*, and 2538.6-keV,* $\mathbf{4^-}$ *states*

The de-excitation γ rays from these levels of 1354.4 and 1357.3 keV, respectively, are partly overlapping (Fig. 14), but χ^2 analysis of the 1357-keV line at forward angles and of the 1354-keV line at backward angles gave unambiguous results.

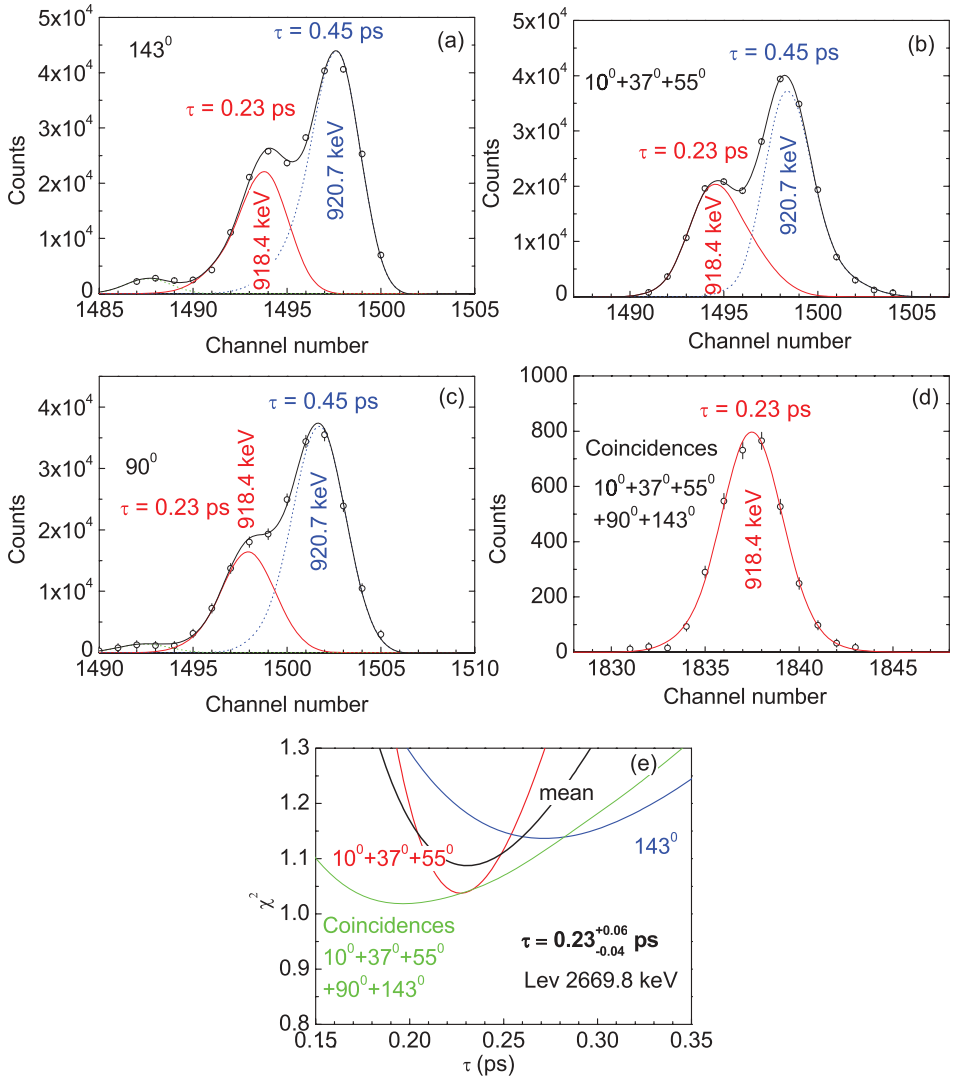

FIG. 16. (Color online) Same as Fig. 11, for the 918.4-keV transition from the 2669.8-keV state. There are two contaminating transitions in the singles spectra; the one with 920.7-keV energy also presents a Doppler effect. The transition is clean in the coincidence spectrum. The lifetime was extracted from a combined analysis of all these spectra.

The error of the 2538.6-keV level lifetime is large owing to both the small Doppler effect and the relatively low statistics.

5. *The 2600.8-keV,* I = 3*; 2603.7-keV,* J = 4*; and 3166.4-keV states*

The de-exciting transitions of 1419.2, 1422.4, and 1415.5 keV, respectively, form a multiplet of partly overlapping lines, together with a contaminating line at 1409 keV (Fig. 15). Despite this complicated situation, a careful analysis, simultaneously considering both the backward- and the forward-angle spectra, provided results for all three levels. The 1422.4-keV line is a doublet with an 81% contribution from the 2603.7-keV level of interest and a 19% contribution from the 2679.4-keV level, which has a known lifetime of 635^{+125}_{-40} fs [4]. Because the χ^2 analysis gives an effective value $\tau_{\text{eff}} = 465^{+50}_{-35}$ fs, the calculated lifetime for the 2603.7-keV level is $\langle\tau\rangle \geqslant 425^{+65}_{-40}$ fs. The lifetimes of the 2603.7- and 3166.4-keV states are new. For the 2600.8-keV level the present result is more precise than that in Ref. [4].

6. *The 2669.8-keV,* 8^+_1 *state*

In the singles spectra, the 918.4-keV transition from this state is contaminated by two lines, the one with the higher energy, 920.7 keV, also presenting a Doppler effect (Fig. 16). Nevertheless, this line is clean in coincidence, although the χ^2 analysis of that spectrum is less sensitive. A reliable result was obtained by analyzing both the singles and the coincidence spectra. A lifetime of $0.31^{+0.04}_{-0.03}$ ps was obtained without considering the cascade feeding of this level. With a 30% cascade feeding from the levels at 3099.4, 3290.9, 3334.7, 3382.0, 3415.3, 3626.2, and 3684.9 keV, one gets a lifetime of 230^{+60}_{-40} fs.

7. *The 2679.4-keV,* 4^+ *state*

The 2116.0-keV transition from this level has the highest energy and Doppler effect analyzed in this work. Therefore, despite its rather poor statistics and the presence of a contaminant, the analysis (Fig. 17) provides a reasonable accuracy: $\tau = 650^{+150}_{-100}$ fs. The result in Ref. [4] is 599^{+257}_{-110} fs,

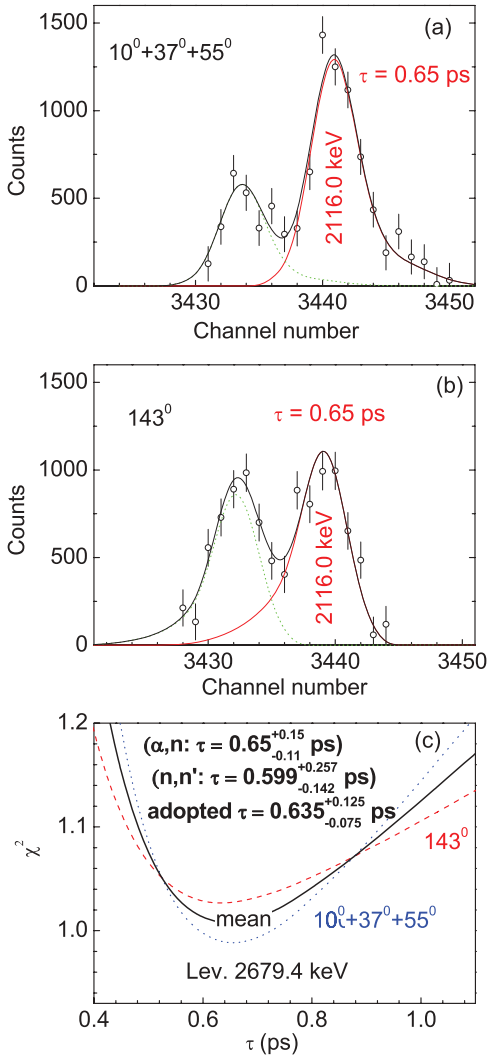

FIG. 17. (Color online) Same as Fig. 11, for the 2116.0-keV transition of the 2679.4-keV level, which is close to a contaminating transition of lower energy. The lifetime measured with the (n,n') reaction [4] is also shown for comparison (c).

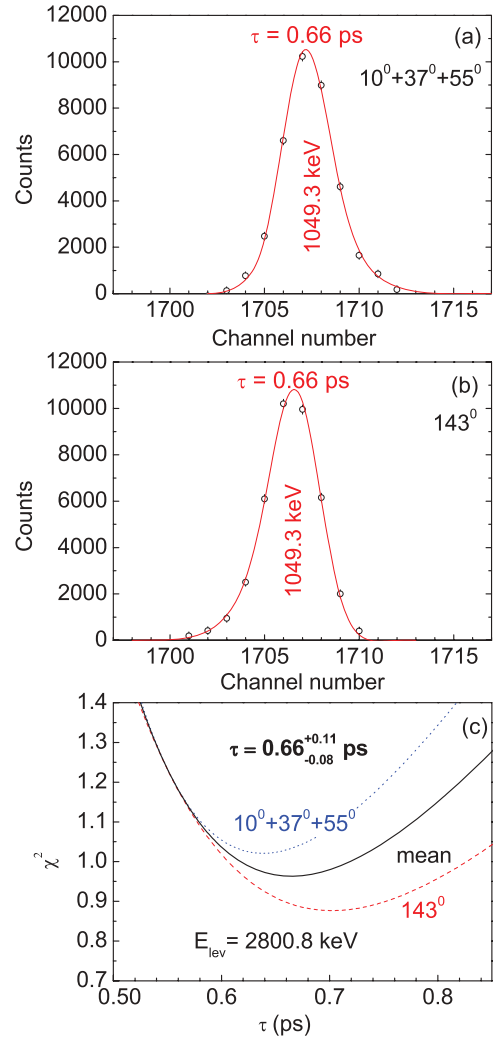

FIG. 18. (Color online) Line-shape analysis of the 1049.3-keV transition from the 2800.8-keV level.

with a slightly larger error, therefore we adopt the value $\tau = 635^{+125}_{-110}$ fs (Table III).

8. The 2800.8-keV, 7⁻ state

This is a rare example where the de-exciting transition, of 1049.3 keV, is very clean in the singles spectra (Fig. 18). Therefore, despite the rather small Doppler effect, the χ^2 analysis provided a result with about 15% accuracy: $\tau = 660^{+110}_{-80}$ fs.

9. The 2810.0-keV, $I^\pi = 4^+$, 3, and 2816.7-keV, I = 4, 5, states

Figure 19 shows the de-exciting transitions of 1628.6 and 1635.9 keV, respectively, which strongly overlap the Doppler broadened 1632.9-keV transition from the 3^- level at 2196.8 keV. In addition, the 1635.9-keV line also overlaps with the 1639.8-keV line from the 2203.8-keV ($I = 1$) level, which shows a large Doppler effect. Figure 19 shows another small impurity peak at 1645 keV, having an instrumental shape only. All five of these lines were considered in the analysis. Fortunately, the lines at 1632.9 and 1639.8 keV could be taken into account by calculating them with fixed lifetimes of 0.15 and 0.18 ps, respectively, which were determined with good accuracy in Ref. [4], and properly taking into account the feedings of the corresponding levels (Table I). The lifetime of the 2810.0-keV level was determined with about 10% accuracy, $\tau = 320^{+27}_{-22}$ fs, while that of the 2816.7-keV level was determined with larger errors, $\tau = 1.22^{+0.39}_{-0.23}$ ps, but was considerably more precise than the rough estimation in Ref. [4], $0.903^{+1.150}_{-0.340}$ ps.

10. The 2878.3-keV state

The de-exciting transition of 1127.4 keV from this newly assigned excited level belongs to a complicated multiplet in

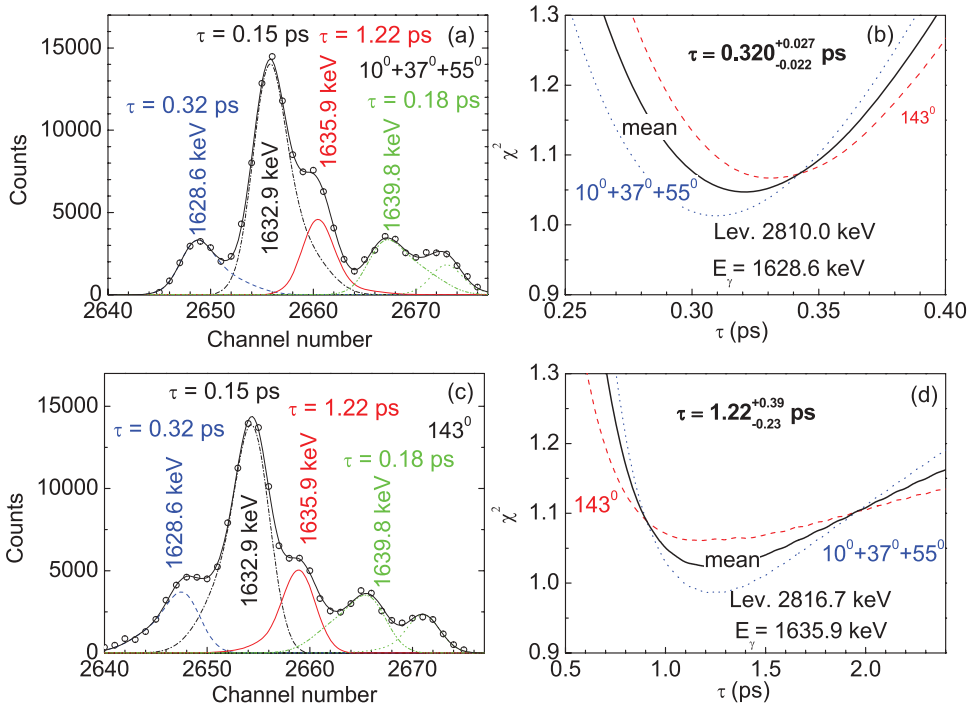

FIG. 19. (Color online) Same as Fig. 11, showing the analysis of a complicated multiplet of five lines. The transitions of 1632.9 keV (from the 2196.8-keV level) and 1639.8 keV (from the 2203.8-keV level) were calculated with their known lifetimes from Ref. [4], while the lifetimes of the 2810.0-keV level (de-exciting through the 1628.6-keV line) and the 2816.7-keV level (1635.9-keV line) were determined from the fit. The contaminating peak at the right had only instrumental shape.

the singles spectra. Nevertheless, the coincidence spectra were clean (Fig. 20) and could be used to extract a value $\tau = 580^{+120}_{-80}$ fs for this level.

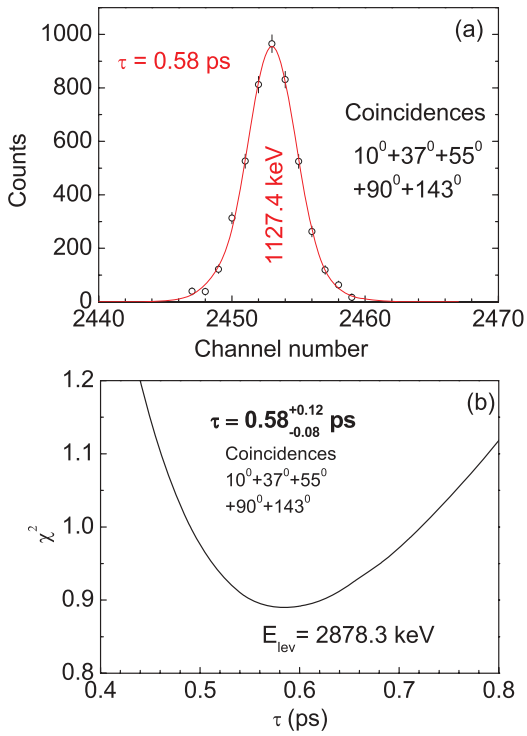

FIG. 20. (Color online) Line-shape analysis of the 1127.4-keV transition from the 2878.3-keV state. This line could be seen cleanly only in the coincidence spectrum.

11. The 2913.5-keV, 8^+ state

The corresponding transition, 1161.8 keV, exhibits a small Doppler broadening and is disturbed by two contaminating lines (Fig. 21). Fortunately, the analysis of forward, backward, and 90° angle spectra allowed us to establish the position of these peaks and to deduce that their shape was purely instrumental. In the forward angle spectrum the influence of the contaminants is smaller and the χ^2 analysis was sensitive enough to provide a reasonable lifetime estimation of $\tau = 630^{+140}_{-90}$ fs (taking into account the feeding of this level from the one at 3210.9 keV).

12. The 3324.3-keV state

Its 1573.4-keV γ ray is strongly contaminated by the 1576.8-keV line from the 2758.3-keV level. Two additional lines with instrumental shapes had to be considered in the analysis (Fig. 22). Fortunately, in the analysis of this peak, knowledge of the well-determined lifetime of the 2758.3-keV level, 0.19 ps [4], was beneficial. The value obtained is $\tau = 630^{+260}_{-180}$ fs.

F. Monte Carlo simulation of the reduced electromagnetic transition probability distributions

In many cases the errors of the lifetimes, branching ratios, and mixing ratios δ are quite large. Under these conditions transformation of these errors into the finally deduced reduced transition probabilities like $B(M1)$, $B(E2)$, and $B(E1)$ using the error propagation law underestimates their uncertainties. The best way to avoid this is to investigate the resulting

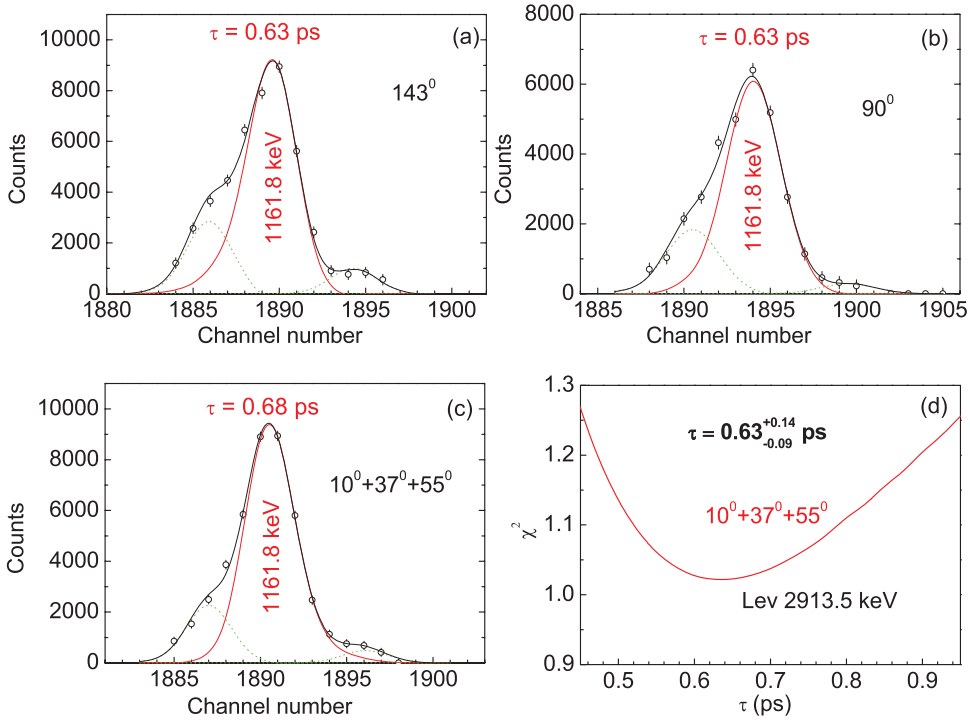

FIG. 21. (Color online) Lineshape analysis of the 1161.8-keV transition from the 2913.5-keV state. Two contaminating transitions were found, with only an instrumental line shape.

probability distribution with Monte Carlo simulations. This approach was proposed in Ref. [32] and applied to pure $M1$ transitions in dipole bands [11,32–34], as well as to pure $E2$ transitions in quadrupole bands [8–10]. In this work the corresponding program has been extended to mixed $E2/M1$ transitions, taking into account the fact that the errors in the mixing ratios are usually large and asymmetric.

The central values for the lifetimes τ in Table II correspond to the maximum of the probability distributions $P(\tau)$, which have been approximated by Gaussian functions with equal ($\pm\sigma_\tau$) or different ($+\sigma_+$, $-\sigma_-$) Gaussian parameters and do not take into account the error connected with the stopping power uncertainties. The errors in the calculated values of the transition probabilities $B(\sigma,\lambda)$ presented in Table III include this contribution. Namely, the probability of the deviation of the electronic and nuclear stopping power correction factors from an expected central value is assumed to be Gaussian distributed with a parameter $\sigma_{\rm syst}(\tau) = r\tau$, where $r = 15\%$ is the systematic relative error, regarded as a scale factor for τ. Even in the case of symmetrical errors in the lifetime, applying the correction owing to stopping power uncertainty results in a complex, non-Gaussian distribution for the lifetime. In the general case of an asymmetric initial distribution, only a Monte Carlo procedure is possible to correctly evaluate the errors. The calculated distribution $P_{\rm corr}(\tau)$ is characterized by new errors that are defined by the bounds of the 68% confidence interval. Figure 23(a) shows as an example the case of the $E_x = 2816.7$ keV level. The $B(M1)$ and $B(E2)$ values were calculated according to $B(M1) \sim [K_{\rm br}(I_i)/\tau][1/(1+\delta^2)]$ and $B(E2) \sim [K_{\rm br}(I_i)/\tau][\delta^2/(1+\delta^2)]$, where $K_{\rm br} = I_i/\Sigma I_n$ is the branching ratio coefficient, and I_n are the intensities of all the outgoing transitions, supposed to be symmetrically Gaussian distributed, whereas δ has an asymmetric Gaussian distribution and τ is distributed as $P_{\rm corr}(\tau)$. After the Monte Carlo calculation of the $B(\sigma,\lambda)$ probability distributions, the most probable $B(\sigma,\lambda)$ value and its two errors (Δ_+ and Δ_-) evaluated for the 68% level of confidence, are presented in the $B(\sigma,\lambda)$ column in Table III. The median value of $B(\sigma,\lambda)$ (last column) is calculated from these distributions. Figures 23(b) and 23(c) show examples of the $B(M1)$ and $B(E2)$ distributions for the 907.0-keV transition of the $E_x = 2816.7$ keV level, respectively, where the δ interval includes the zero value.

IV. CONCLUSIONS

In this work we have analyzed the possibilities of DSAM analysis of Doppler broadened line shapes obtained following an $(\alpha,n\gamma)$ reaction. Experimental measurements have been performed with the ^{119}Sn$(\alpha,n)^{122}$Te reaction on a thick target, at 15.0-MeV incident energy. Singles and $\gamma\gamma$ coincidence spectra were measured at the angles 10°, 37°, 55°, 90°, and 143°. A complex level and γ-ray decay scheme has been observed in ^{122}Te up to spin $10\hbar$. Thus, the (α,n) reaction occupies a distinct place between heavy-ion-induced reactions and (p,n) or (n,n') reactions.

A careful analysis of the Doppler broadened line shapes observed both in singles and in coincidence was performed with Monte Carlo simulations that take into account the reaction kinematics, the compound nucleus formation, the de-excitation process of the entry states, the slowing-down of the recoils, the energy response, and the geometry of the detection setup, aiming at the determination of the lifetimes

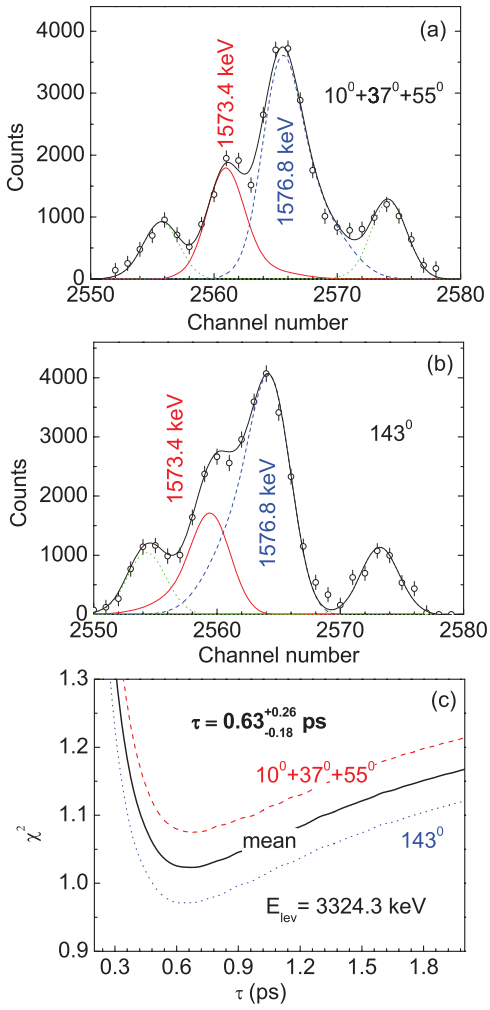

FIG. 22. (Color online) Line-shape analysis of the 1573.4-keV transition from the 3324.3-keV state. The line shape of the 1576.8-keV line could be calculated with the known lifetime of its 2758.3-keV level [4]. The other two, contaminating lines have only instrumental line shapes.

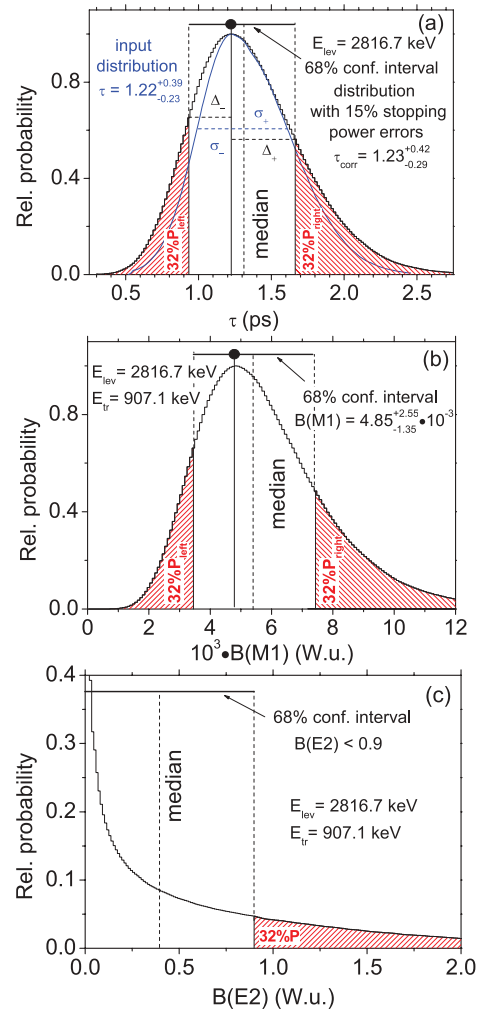

FIG. 23. (Color online) Illustration of the Monte Carlo simulations (Sec. III F) of the probability distributions used to deduce the $B(\sigma,\lambda)$ values (Table III). (a) Probability distribution for the lifetime of the $E_x = 2816.7$ keV level, with and without uncertainty in the stopping power. (b, c) Probability distributions for the $B(M1)$ and $B(E2)$ transition rates of the 907.0-keV transition from the same state, which consider the asymmetric errors of both the lifetime and the mixing ratio (see Tables I and III). The extracted $B(\sigma,\lambda)$ values (listed in Table III) are also shown.

of the excited states. The study shows that although the recoil velocities in this reaction are modest ($v/c \sim 0.3\%$), resulting in Doppler broadening of the γ rays comparable to, or just somewhat larger than, the FWHM energy resolution of the detector, a rather meaningful DSAM analysis can be performed provided that the instrumental response of the detector and the feeding times of the studied levels are properly taken into account. It has been shown that a good calibration of the side feeding time patterns can be obtained by using some existing, reliable lifetime values, in our case known from a $(n,n'\gamma)$ reaction experiment where the side feeding time problem was absent [4]. As a result, for a number of levels with excitation between 1.9 and 3.3 MeV, we either determined the lifetime for the first time or were able to provide a more precise value. We have also presented a Monte Carlo procedure to correctly calculate the electromagnetic transition rates from the usual data (lifetimes, branching ratios, mixing ratios), which may have large and asymmetric errors. The results obtained validate the use of Monte Carlo DSAM analysis of the (α,n) reaction for precise lifetime determinations, in the domain between $\sim$0.05 and $\sim$1.5 ps, for low- and medium-spin states with the (α,n) reaction.

ACKNOWLEDGMENTS

This work was partly supported by the Romanian Ministry for Education and Research under Research Project Nos. 71-042/2007, 71-051/2007, 67CP/I/2007, PN 09370105/2009, IDEI-181/2007, and IDEI-48/2007.

[1] T. K. Alexander and J. S. Foster, *Advances in Nuclear Physics*, edited by M. Baranger and E. Vogt (Plenum Press, New York, London, 1978), Vol. 10, p. 197.

[2] A. Dewald, R. Reinhard, J. Panqueva, K. O. Zell, and P. von Brentano, Z. Phys. A **315**, 77 (1984).

[3] I. Căta-Danil, D. Filipescu, M. Ivaşcu, D. Bucurescu, N. V. Zamfir, T. Glodariu, L. Stroe, G. Căta-Danil, D. G. Ghiţă, C. Mihai, G. Suliman, and T. Sava, Phys. Rev. C **78**, 035803 (2008).

[4] S. F. Hicks, G. K. Alexander, C. A. Aubin, M. C. Burns, C. J. Collard, M. M. Walbran, J. R. Vanhoy, E. Jensen, P. E. Garrett, M. Kadi, A. Martin, N. Warr, and S. W. Yates, Phys. Rev. C **71**, 034307 (2005).

[5] T. Tamura, Nucl. Data Sheets **108**, 455 (2007).

[6] J. Srebrny, Ch. Droste, T. Morek, K. Starosta, A. A. Wasilewski, A. A. Pasternak, E. O. Podsvirova, Yu. N. Lobach, G. H. Hagemann, S. Juutinen, M. Piiparinen, S. Tormanen, and A. Virtanen, Nucl. Phys. A **683**, 21 (2001).

[7] R. M. Lieder, A. A. Pasternak, E. O. Podsvirova, A. D. Efimov, V. M. Mikhajlov, R. Wyss, Ts. Venkova, W. Gast, H. M. Jager, L. Mihailescu, D. Bazzacco, S. Lunardi, R. Menegazzo, C. Rossi Alvarez, G. de Angelis, D. R. Napoli, T. Rzaca-Urban, and A. Dewald, Eur. Phys. J. A **21**, 37 (2004).

[8] E. Grodner, A. A. Pasternak, Ch. Droste, T. Morek, J. Srebrny, J. Kownacki, W. Plociennik, A. A. Wasilewski, M. Kowalczyk, M. Kisielinski, R. Kaczarowski, E. Ruchowska, A. Kordyasz, and M. Wolinska, Eur. Phys. J. A **27**, 325 (2006).

[9] E. O. Lieder, A. A. Pasternak, R. M. Lieder, V. M. Mikhajlov, B. G. Carlsson, I. Ragnarsson, W. Gast, Ts. Venkova, T. Morek, S. Chmel, G. de Angelis, D. R. Napoli, A. Gadea, D. Bazzacco, R. Menegazzo, S. Lunardi, W. Urban, Ch. Droste, T. Rzaca-Urban, G. Duchene, and A. Dewald, Eur. Phys. J. A **35**, 135 (2008).

[10] I. Sankowska, Ch. Droste, E. Grodner, T. Morek, J. Srebrny, A. A. Pasternak, J. Kownacki, P. Napiorkowski, S. G. Rohozinski, M. Kowalczyk, M. Kisielinski, R. Kaczarowski, and E. Ruchowska, Eur. Phys. J. A **37**, 169 (2008).

[11] A. A. Pasternak, E. O. Lieder, R. M. Lieder, S. Chmel, W. Gast, Ts. Venkova, G. de Angelis, D. R. Napoli, A. Gadea, D. Bazzacco, R. Menegazzo, S. Lunardi, and G. Duchene, Eur. Phys. J. A **37**, 279 (2008).

[12] A. A. Pasternak, J. Srebrny, A. D. Efimov, V. M. Mikhajlov, E. O. Podsvirova, Ch. Droste, T. Morek, S. Juutinen, G. B. Hagemann, M. Piiparinen, S. Türmänen, and A. Virtanen, Eur. Phys. J. A **13**, 435 (2002).

[13] A. A. Pasternak, Y. Sasaki, A. D. Efimov, V. M. Mikhajlov, T. Hayakawa, Y. Toh, M. Oshima, Y. Hatsukawa, J. Katakura, N. Shinohara, Z. Liu, and K. Furuno, Eur. Phys. J. A **9**, 293 (2000).

[14] H. P. Helmeister, K. P. Lieb, and W. Muller, Nucl. Phys. A **307**, 515 (1978).

[15] J. Urban, D. G. Sarantites, and L. L. Rutledge, Nucl. Instrum. Methods **126**, 49 (1975).

[16] D. Ward *et al.*, Nucl. Phys. A **332**, 433 (1979).

[17] Yu. N. Lobach, A. A. Pasternak, J. Srebrny, Ch. Droste, G. H. Hagemann, S. Juutinen, T. Morek, M. Piiparinen, E. O. Podsvirova, S. Türmänen, K. Starosta, A. Virtanen, and A. Wasilewski, Acta Phys. Pol. B **30**, 1273 (1999).

[18] R. Schwengner, G. Winter, J. Döring, L. Funke, P. Kemnitz, E. Will, A. E. Sobov, A. D. Efimov, M. F. Kudojarov, I. Kh. Lemberg, A. S. Mishin, A. A. Pasternak, L. A. Rassadin, and I. N. Chugunov, Z. Phys. A **326**, 287 (1987).

[19] J. Adam, M. Honusek, A. Spalek, D. N. Dinikov, A. D. Efimov, M. F. Kodujarov, I. Kh. Lemberg, A. A. Pasternak, O. K. Vorov, and U. Y. Zhovliev, Z. Phys. A **332**, 143 (1989).

[20] L. Kübler, Yu. N. Lobach, V. V. Trishin, A. A. Pasternak, M. F. Kudojarov, H. Prade, J. Reif, R. Schwengner, G. Winter, J. Blomqvist, and J. Döring, Z. Phys. A **358**, 303 (1997).

[21] J. Mrazek, M. Honusek, A. Spalek, J. Bielcik, J. Slivova, and A. A. Pasternak, Acta Phys. Pol. B **29**, 433 (1998).

[22] Yu. N. Lobach, L. Kübler, R. Schwengner, and A. A. Pasternak, Phys. Rev. C **59**, 1975 (1999).

[23] J. Mrazek, M. Honusek, A. Spalek, J. Bielcik, J. Slivova, J. Adam, and A. A. Pasternak, Eur. Phys. J. A **5**, 399 (1999).

[24] Yu. N. Lobach, A. D. Efimov, and A. A. Pasternak, Eur. Phys. J. A **6**, 131 (1999).

[25] E. Grodner *et al.*, Phys. Rev. Lett. **97**, 172501 (2006).

[26] K. B. Winterbon, Nucl. Phys. A **246**, 293 (1975).

[27] I. K. Lemberg and A. A. Pasternak, Nucl. Instrum. Methods **140**, 71 (1977).

[28] E. O. Lieder, A. A. Pasternak, R. M. Lieder, R. A. Bark, E. A. Lawrie, J. J. Lawrie, S. M. Mullins, S. Murray, S. S. Ntshangase, P. Papka, N. Kheswa, W. J. Przybylowicz, P. T. Sechogela, and K. O. Zell, Nucl. Instrum. Methods Phys. Res. Sect. A **607**, 591 (2009).

[29] J. Kopecky, in *Reference Input Parameter Library (RIPL). Handbook for Calculations of Nuclear Reaction Data, IAEA-TECDOC-1034* (IAEA, Vienna, 1998), Chap 6; http://www.nds.iaea.or.at/ripl/.

[30] S. S. Dietrich and B. L. Berman, At. Data Nucl. Data Tables **38**, 199 (1988).

[31] J. Kopecky and M. Uhl, Report ENEA/NSC/Doc(95)1, p. 119.

[32] E. O. Podsirova, R. M. Lieder, A. A. Pasternak, S. Chmel, W. Gast, Ts. Venkova, H. M. Jäger, L. Mihăilescu, G. de Angelis, D. Napoli, A. Gadea, D. Bazzacco, R. Menegazzo, S. Lunardi, W. Urban, Ch. Droste, T. Morek, T. Rzaca-Urban, and G. Duchene, Eur. Phys. J. A **21**, 1 (2004).

[33] A. A. Pasternak, E. O. Podsirova, R. M. Lieder, S. Chmel, W. Gast, Ts. Venkova, H. M. Jäger, L. Mihăilescu, G. de Angelis, D. Napoli, A. Gadea, D. Bazzacco, R. Menegazzo, S. Lunardi, W. Urban, Ch. Droste, T. Morek, T. Rzaca-Urban, and G. Duchene, Eur. Phys. J. A **23**, 191 (2005).

[34] E. Grodner, J. Srebrny, A. A. Pasternak, J. Zalewska, T. Morek, Ch. Droste, J. Mierzejewski, M. Kowalczyk, J. Kownacki, M. Kisielinski, S. G. Rohozinski, T. Koike, K. Starosta, A. Kordyasz, P. J. Napiorkowski, M. Wolinska-Cichocka, E. Ruchowska, W. Plociennik, and J. Perkowski, Phys. Rev. Lett. **97**, 172501 (2006).